Genetic ablation of RhoA in adult microglia causes synapse and neuronal loss

Renato Socodato[1,*], Camila C. Portugal[1,*], Teresa Canedo[2], Joana F. Henriques[2], Sandra H. Vaz[10,11], João Magalhães[2], Cátia M. Silva[1], Filipa I. Baptista[3,5,6], Renata L. Alves[2,8], José Nogueira[1], Vanessa Coelho-Santos[4,5,6], Ana Paula Silva[4,5,6], Roberto Paes-de-Carvalho[7], Ana Magalhães[2] , Teresa Summavielle[2], Cord Brakebusch[9], Ana M. Sebastião[10,11], António F. Ambrósio[3,5,6] and João B. Relvas[1,#]

[1]Glial Cell Biology Lab, Instituto de Investigac□ão e Inovac□ão em Saúde and Instituto de Biologia Molecular e Celular, Universidade do Porto, Porto, Portugal.

[2]Addiction Biology Lab, Instituto de Investigac□ão e Inovac□ão em Saúde and Instituto de Biologia Molecular e Celular, Universidade do Porto, Porto, Portugal.

[3]Institute for Biomedical Imaging and Life Sciences, IBILI, Faculty of Medicine, University of Coimbra, Coimbra, Portugal.

[4]Institute of Pharmacology and Experimental Therapeutics, Faculty of Medicine, University of Coimbra, Coimbra, Portugal

[5]Association for Innovation and Biomedical Research on Light and Image (AIBILI).

[6]CNC.IBILI Consortium, University of Coimbra, Coimbra, Portugal.

[7]Department of Neurobiology and Program of Neurosciences, Institute of Biology, Fluminense Federal University, Niterói, Brazil.

[8]Faculty of Psychology and Education Sciences, University of Porto, Porto, Portugal.

[9]Molecular Pathology Section, BRIC, Københavns Biocenter, Copenhagen, Denmark.

[10]Instituto de Farmacologia e Neurociências, Faculdade de Medicina, Universidade de Lisboa, Lisboa, Portugal.

[11]Instituto de Medicina Molecular, Faculdade de Medicina, Universidade de Lisboa, Lisboa, Portugal.

#Corresponding author: João Bettencourt Relvas (jbrelvas@ibmc.up.pt)

*Renato Socodato and Camila C. Portugal contributed equally to this manuscript.

Summary

Microglia, the resident myeloid cells of the central nervous system parenchyma, are critical for brain functioning in health and disease. Here, using tissue-specific conditional gene targeting in mice, we show an essential role for the small GTPase RhoA in regulating microglia homeostasis and brain pathology. We reveal that in the absence of brain disease or any insult, the microglia-specific ablation of RhoA disrupted the quiescence of adult microglia leading to their activation, which culminated in astrogliosis, inflammation, synapse and neuronal loss, impairment of long-term potentiation and memory deficts. RhoA exerted its microglial homeostatic functions by sustaining C-terminal Src kinase (Csk) negative regulation of Src tyrosine kinase activity. Accordingly, inhibition of Src with a clinically-relevant inhibior prevented microglia deregulation and synapse loss restoring the memory performance of mice with microglia-specific ablation of RhoA. Overall, loss of RhoA in adult brain microglia leads to a neurodegenerative-like pathology mediated by deregulated microglial activation.

Keywords: astrocytes, behaviour, inflammation, LTP, RhoGTPase, Src tyrosine kinase

Introduction

Microglia are yolk sack-derived myeloid cells that populate the early nervous system rudiment (Ginhoux et al., 2010). Microglia are an autonomous cell population, ontologically and transcriptomically distinct from other tissue-resident myeloid cells and circulating monocytes (Ginhoux and Guilliams, 2016). Under physiological conditions, microglia continuously extend and retract their cellular processes, monitoring the central nervous system (CNS) parenchyma for tissue damage or infections and checking the functional status of brain synapses (Crotti and Ransohoff, 2016). Following CNS tissue damage or infection, microglia become activate, changing their morphology into a more amoeboid shape, and function as innate immune cells clearing cell debris and restoring homeostasis (Crotti and Ransohoff, 2016). Although attempting to repair injuries to the parenchyma, exacerbation or prolonged microglial activation may impair neuronal survival in neuropathologies or delay CNS recovery after insults (Gomez-Nicola et al., 2013; Rice et al., 2015; Spangenberg et al., 2016). Such detrimental role for microglia is attributed to their sustained proinflammatory polarization, which is characterized by increased production and release of proinflammatory cytokines (IL-1β and TNF), nitric oxide (NO), reactive oxygen species (ROS) and glutamate (Block et al., 2007).

Dynamic reorganization of the cytoskeleton is likely to underlie microglial function(s) at the steady state and during activation. In line with this, proinflammatory microglial polarization is associated with profound changes in microglia morphology requiring cytoskeleton reorganization (abd-el-Basset and Fedoroff, 1995; Kaur, 1997). The GTPases of the Rho subfamily, from which RhoA, Rac1 and cdc42 are the founding and most well studied members, are key orchestrators of cytoskeleton dynamics (Bustelo et al., 2007) and are therefore well positioned to regulate microglia activation. These molecules not only regulate signaling pathways linking extracellular stimuli to the

assembly and organization of the actin cytoskeleton but also control microtubule dynamics, cell polarity, membrane trafficking and gene transcription in different cell types (Bustelo et al., 2007; Hodge and Ridley, 2016; Ridley, 2015). Typical GTPases function as binary switches by cycling between a GDP-bound inactive “off” state and a GTP-bound active “on” state in which they can directly interact with downstream effectors to regulate different cell functions (Bustelo et al., 2007; Hodge and Ridley, 2016; Ridley, 2015). Although the molecular design of the Rho GTPase switch is relatively simple, its spatiotemporal activity is under the tight control of regulatory proteins (Hodge and Ridley, 2016).

RhoGTPases are extensively expressed in the CNS, play important roles during its development, and dysregulation of their expression and/or activity is associated with different neuropsychiatric disorders (DeGeer and Lamarche-Vane, 2013; Govek et al., 2005; Stankiewicz and Linseman, 2014). The ubiquitously expressed RhoA itself controls the functions of different CNS cell types *in vivo* (Cappello et al., 2012; Herzog et al., 2011; Katayama et al., 2011; Zhou and Zheng, 2013) and changes in its activity or in the activities of its effectors are implicated in the pathophysiology of several CNS diseases, including stroke, Alzheimer´s and Parkinson´s disease and amyotrophic lateral sclerosis (DeGeer and Lamarche-Vane, 2013; Droppelmann et al., 2014).

Microglia dysregulation and neuroinflammation are hallmarks of the abovementioned CNS pathologies (Gomez-Nicola and Perry, 2015; Perry and Holmes, 2014) and suppression of microglia activation and/or microglia-mediated inflammation is considered a promising strategy in fighting neurodegenerative disorders (Dheen et al., 2007). In this context, the pharmacological inhibition of the RhoA effector Rho-kinase (ROCK) by Y27632 or fasudil attenuates microglia activation, promoting some functional recovery in animal models for different neurological conditions (Chen et al., 2013; Chong

et al., 2016; Mueller et al., 2005). Because RhoA is likely to exert its control over microglia through several other downstream effectors besides ROCK, which activation can also be regulated independently of RhoA (Julian and Olson, 2014), these studies are not very informative concerning RhoA regulation of microglial function. In addition, Y27632 and fasudil are not cell specific and have substantial off-target effects, making it difficult to attribute any phenotype solely to the inhibition of ROCK (Vigil and Der, 2013).

Here, using tamoxifen-inducible conditional gene ablation in mice, we investigated for the first time the *bona fide* function of RhoA in microglia. This methodology allowed us to examine rigorously the requirements for this RhoGTPase in microglia under physiological conditions (at the steady state). Our data revealed a critical role for RhoA in controlling the homeostasis of microglia in the adult brain. *In vivo* ablation of RhoA specifically in microglia led to dysregulation of brain resident microglia, astrogliosis, angiogenesis, neuroinflammation, impairment of long-term synaptic plasticity and cognitive deficits with loss of synapses and neuronal cell death. We also show that loss of RhoA activity in microglia is required for proinflammatory microglia polarization triggered by LPS or hypoxia and that RhoA-mediated microglia deregulation relied on the decrease of Csk expression and subsequent overactivation of Src. Overall, our data not only uncover novel and critical roles for RhoA in regulating microglia under physiological conditions but also show that microglia dysfunction can, in a cell autonomous fashion, initiate cellular and molecular mechanisms leading to a neurodegenerative-like disease.

Results

Conditional ablation of *RhoA* in microglia

To conditionally ablate *RhoA* in microglia, we used mice expressing both EYFP and tamoxifen-inducible Cre recombinase (Cre^{ER}) under the endogenous regulation of Cx3cr1 promoter **(Fig. 1A).** This transgene is transcriptionally active in microglia **(Suppl. Fig. 1A)** and in the brains of $Cx3cr1^{CreER\text{-}EYFP}$ mice, a population of $EYFP^+$ cells corresponded almost exclusively to the resident survailling microglia, which are a population of $Ly6C^{low}CD45^{mid}CD11b^+$ cells (**Suppl. Fig. 1B)**. In microglia-specific RhoA mutant (RhoA cKO) mice, Cre translocates to the nucleus following administration of tamoxifen, allowing us to adjust the timing of microglial *RhoA* gene inactivation to our experimental requirements. We thus administered tamoxifen by oral gavage to control and RhoA cKO mice between P26-P28 and analyzed their brains at P65-70 **(Fig. 1B)**. qRT-PCR analysis of FACS-sorted Cx3cr1-$EYFP^+$ cells showed a very substantial reduction of *RhoA* transcripts in RhoA cKO microglia compared with those from control microglia **(Fig 1C).**

RhoA is a critical regulator of microglia homeostasis in the adult brain

We then evaluated the requirement of RhoA for microglia homeostasis in the adult brain at the steady state. Using FACS analysis**,** we observed a decrease in the frequency of microglia ($Ly6C^{low}CD45^{mid}CD11b^+$) in the brains of RhoA cKO mice when compared with the brains of control littermates (**Fig. 1D**). The percentage of brain $CD11b^+CD45^{high}$ cells, including the subpopulations of $Ly6C^{low}$ or $Ly6C^{high}$ macrophages, were comparable in the brains of RhoA cKO and control animals (**Fig. 1D**).

Because Cx3cr1 is also expressed on peripheral organs (Jung et al., 2000),

some degree of Cre-mediated recombination of *RhoA* floxed alleles is expected to occur outside the CNS in RhoA cKO mice after tamoxifen administration (Goldmann et al., 2013; Parkhurst et al., 2013). FACS analysis of blood, spleen and liver 35 days posttamoxifen revealed that the percentage of different $CD45^{+}$ myeloid populations were similar between RhoA cKO and control littermates (**Suppl. Figs. 1C-E**), confirming, as expected, that the phenotype observed in RhoA cKO mice was restricted to the CNS compartment and specific for the resident microglial population. Immunohistochemistry with Iba1 on tissue sections obtained from the brains of control and RhoA cKO revealed that mutant microglia were dystrophic, being smaller and less ramified when compared with control microglia (**Suppl. Fig. 2A).**

The decrease of microglial numbers and the changes in their morphology are indicative of dysruption of microglia quiescence in RhoA cKO brains. In line with this, by qRT-PCR we detected a significant decrease in the transcript levels of the microglia maintenance genes *csfr1* and *tgfβr1* and a reduction in transcript levels of the microglia signature genes *p2ry12*, *mertk*, *gpr34*, and *pros1* (Butovsky et al., 2014) in RhoA cKO brains compared to those in controls (**Fig. 1E**). Because the expression of these genes strongly correlates with microglial homeostatic functions (Butovsky et al., 2014) and are altered upon pathological conditions, including inflammation (Greter et al., 2015; Healy et al., 2016; Preissler et al., 2015), we concluded that RhoA is required for microglia homeostasis in the adult brain at the steady state.

It is expected that disrupting microglia quiescence may lead to microglia activation. Thus, we evaluated the activation of microglia after depleting RhoA. Whereas RhoA cKO microglia contrained increased mRNA transcripts for the proinflammatory cytokines *Tnf* and *IL-1β* when compared to control microglia, the mRNA levels of *IL-6* was similar between CT and RhoA cKO microglia (**Fig. 1F**). During the inflammatory

response, proinflammatory cytokine production is NF-kB dependent (Lawrence, 2009). Accordingly, knocking down (KD) RhoA in microglia using shRNA **(validation in Suppl. Fig. 2B)** resulted in nuclear accumulation of the GFP-tagged p65 subunit of the NF-□B (**Suppl. Fig. 2C**), reporting its activation, and in increased release of TNF (**Suppl. Fig. 2D**). Depletion of RhoA also gave rise to enhanced glutamate release and ROS production in living microglia, measured using FRET-based biosensors (**Suppl. Figs. 2E and F, respectively**).

Phagocytosis is also a phenotypic feature of microglia activation and we asked whether RhoA would also impact microglial phagocytosis. We found that the phagocytic capacity of RhoA KD microglia was significtanly higher than control microglia (**Fig. 1G**). On the other hand, rapid and specific activation of RhoA using a Rho GTPase chemical inducible dimerization strategy (Inoue et al., 2005) showed that microglia with increased RhoA activity presented decreased phagocytic capacity when compared to control microglia (**Suppl. Fig. 2G**). Here, we concluded that besides regulating microglia inflammatory polarization, RhoA also fine-tunes microglial phagocytosis.

Inflammation in RhoA cKO brains

Microglia activation followed by increased production and release of inflammatory cytokines, glutamate and ROS can adversely impact the surrounding brain tissue (Block et al., 2007). Therefore, we compared the mRNA expression of key inflammation and antioxidant-related genes between RhoA cKO and control brains. Our results showed higher transcript levels of *tnf*, *il-1β*, il-6, reduced levels of *c1qC*, *c1qB*, *cox-2*, *trem2, tspo, tlr4, tlr7, il-18, cd14 and socs3,* and no changes in the levels of *mhc-II*, *tlr2, il-10, cd163*, *irak3*, *mrp14* and *mrp8* in RhoA cKO brains (**Fig. 2A**). We also found lower transcript levels of the antioxidant-related genes *gclc*, *tnxrd1, gsr*, *hmox1 and slc23a2* in RhoA

cKO brains compared with controls (**Fig. 2A**). We then analyzed by Western blotting the amounts of inducible nitric oxide synthase (iNOS), which is a hallmark of brain inflammation (Daulatzai, 2016), on lysates obtained from the brains of RhoA cKO and control mice. Our results showed an increase in the amounts of iNOS (**Fig. 2B**) in RhoA cKO compared with control brains.

Angiogenesis was also observed in the brains of RhoA cKO mice **(Suppl. Figs. 3A and B)**. Immunohistochemistry using an antibody recognizing CD31 (PECAM-1) revealed an increase in the number of endothelial cells **(Suppl. Fig. 3A)** and in blood vessel remodeling **(Suppl. Fig. 3B)** in RhoA cKO brains compared with controls**.** No vessel leakage (extravasation of albumin; **Suppl. Figs. 3C)** or infiltration of $CD4^+$ T-lymphocytes **(Suppl. Figs. 3D)** were observed on tissue sections obtained from the brains of RhoA cKO mice, further suggesting that the blood-brain barrier (BBB) is intact**.** In addition, RhoA cKO brains contained significantly higher number of glial fibrillary acidic protein (GFAP) immunoreactive astrocytes when compared with control brains (**Fig. 2C)**. Taken togheter, these data suggest that the microglia-specific loss of RhoA in the adult brain results in neuroinflammation.

Impairment of long-term potentiation (LTP) in RhoA cKO mice

Because neuroinflammation and increased microglia phagocytosis can adversely affect neuronal functioning and brain plasticity (Brown and Neher, 2014; Di Filippo et al., 2008) we evaluated long and short-term forms of synaptic plasticity in acute hippocampal slices from control and RhoA cKO animals. We first studied LTP by delivering θ-burst stimulation to the Schaffer collateral fibers and recorded the field excitatory post-synaptic potentials (fEPSP) in the *stratum radiatum* of hippocampal CA1 region. θ-burst stimulation of hippocampal slices from control mice led to an initial

enhancement of the fEPSP slope followed by a decrease and stabilization period, but at the end of the recording period fEPSP slope values remained significantly higher than before θ-burst stimulation (**Fig. 3A open circles and 3B gray lines**). In RhoA cKO slices, the same θ-burst stimulation caused only the initial transient increase in fEPSPs slope values, which then decreased progressively towards pre-θ-burst levels at the end of LTP recording (**Fig. 3A purple circles and 3B purple lines**), thus sugesting a marked impairment of LTP in RhoA cKO hippocampus. Accordingly, the magnitude of LTP was substantially higher in hippocampal slices from control than from RhoA cKO mice (**Fig. 3C**).

Post-tetanic potentiation (PTP) was comparable between control and RhoA cKO slices (**Suppl. Fig. 4A**), suggesting that pre-synaptic vesicle fusion events were not altered. Paired-pulse facilitation (PPF), by comparing the ratio between the second and first fEPSP slope values (fEPSP1/fEPSP0), at the Schaffer collateral-CA1 synapse was also similar between RhoA cKO and control slices (**Suppl. Fig. 4B and C**), indicating no deficits in the probability of neurotransmitter release. Putative alterations in basal synaptic efficiency were assessed from input-output (I/O) curves recorded in hippocampal slices from control or RhoA cKO mice. Maximum values obtained by extrapolating the nonlinear fitting of the fEPSP slope against stimulus intensity (**Suppl. Fig. 4D**) or the values of PSFV amplitude against stimulus intensity (**Suppl. Fig. 4E**) were similar in control and RhoA cKO animals. In addition, no differences between genotypes were found when fEPSP slope values were plotted against PSFV amplitude values (**Suppl. Fig. 4F**), suggesting no overt alterations in basal synaptic efficiency.

Altogether these data show that activation of hippocampal microglia after RhoA depletion leads to neuroinflammation, which did not affect pre-synaptically dependent short-term forms of synaptic plasticity or the basal excitability of presynaptic neurons but

induced a marked impairment of LTP.

Deficits in recognition memory in RhoA cKO mice

Alteration of microglia homeostasis, increased phagocytosis, neuroinflammation and LTP impairment in RhoA cKO mice can be detrimental to cognition and behavior. To address this possibility, we compared the performance between RhoA cKO and control mice 30 days after tamoxifen administration in different behavior paradigms, including elevated plus-maze (EPM) to evaluate anxiety-related behaviour; open field (OF) to test general activity levels and gross motor function; and novel object recognition (NOR) to test recognition memory.

OF test did not reveal significant differences in general locomotor or exploratory activity between RhoA cKO and control animals (**Suppl. Fig. 5A-F**). In addition, classical parameters for assessing anxiety-like behavior in the EPM were similar between RhoA cKO and control animals (**Suppl. Fig. 5G**). In the NOR test, RhoA cKO mice spent less time exploring the novel object (**Fig. 3D**) and displayed a significant decrease in the capacity to discriminate the novel object over the familiar object (**Fig. 3E**) compared to controls. Total object exploration time was similar between control and RhoA cKO animals (**Fig. 3F**), thus suggesting that the RhoA-dependent control of microglia homeostasis critically impacts recognition memory in adult mice.

Degenerative pathology in RhoA cKO brains

Memory deficits, impaired synaptic plasticity, astrocytosis, neuroinflammation and microglia activation are phenotypic features commonly found in neurodegenerative disorders. To adress whether depleting RhoA in adult microglia also leads to neurodegeneration we evaluated synapse and neuronal loss in RhoA cKO mice.

Western blot analysis of hippocampal tissue lysates showed that the amounts of the pre-synaptic proteins synapsin-1 and synaptophysin, of the post-synaptic scaffold protein PSD-95, and of the motor protein KIF1A were significantly lower in RhoA cKO than in control hippocampi (**Fig. 4A**). Paralleling this decrease in synaptic proteins, double-labelling immunohistochemistry for vGlut-1 and PSD95 on tissue sections showed that RhoA cKO hippocampus also presented significantly less excitatory synaptic puncta when compared to the controls (**Fig. 4B**), strongly indicating that microglia-specific ablation of RhoA promotes synapse loss.

In addition, RhoA cKO hippocampi contained depositions of hyperphosphorylated Tau, resembling pathological neurofibrillary tangles, whereas control hippocampi were devoid of such depositions (**Fig. 4C**). RhoA cKO hippocampi also presented an increase in the number of cleaved caspase-3 positive cells relative to the controls (**Fig. 4C**). Because neurofibrilary tangles (Gendron and Petrucelli, 2009) and caspase activation are directly correlated with neurodegeneration we evaluated neuronal numbers in RhoA cKO brains. We found significantly lower NeuN-positive neurons both in the hippocampus and in the neocortex of RhoA cKO mice when compared to controls (**Fig. 4E and F)**. Collectively, these data show that ablation of RhoA in adult microglia ultimately leads to phenotypic features of brain disease.

Lasting alterations in RhoA cKO microglia

Some of the phenotypic alterations found in the brains of RhoA cKO mice after 30 days of tamoxifen administration persisted for more than 150 days posttamoxifen administration (**Fig. 5A**). The numbers of microglia in the brains of RhoA cKO mice remained significantly lower when compared to microglia in the brains of control littermates (**Fig. 5B**). Gene expression analysis using qRT-PCR revealed that transcript

levels for the microglial maintenance genes *csfr1* and *tgfβr1* and for the microglial signature genes *p2ry12*, *mertk*, and *pros1* were significantly altered in RhoA cKO brains compared to controls (**Fig. 5C**). Although the mRNA transcript levels for *tnf*, *il-6, il-1β* were similar between control and mutant brains (**Fig. 5C**), transcript levels for other inflammation-related genes such as *c1qC*, *c1qB, il-10*, *il-18*, *tlr7* and *tlr4* also remained significantly altered in RhoA cKO compared to control brains (**Fig. 5C**). The abundance of transcripts for the antioxidant-related genes *tnxrd1*, *gsr*, *hmox1 and slc23a2* were also decreased in the brains of RhoA cKO animals at P180 (**Fig. 5C**). On the other hand, transcript levels for the inflammation-related cytokines *tnf*, *il-1β*, *il-6*, *il-10* and *il-18*, and for the antioxidant-related genes *gclc*, *tnxrd1*, *gsr* and *hmox1* were not altered in the spleen (**Suppl. Fig. 6A**) or in the liver (**Suppl. Fig. 6B**) of RhoA cKO mice compared to control littermates. Collectively, these data suggest that ablation of RhoA in microglia resulted in chronic deregulation of microglia quiescence.

Reduction of RhoA activity is necessary for LPS or hypoxia-induced microglia activation.

Having shown that the specific loss of RhoA in microglia resulted in their activation and in neuroinflammation, we next examined whether reduction of RhoA activity could be triggered exogenously by lipopolysaccharide (LPS) or hypoxia. RhoA pull down assays using cell lysates from rat primary cortical microglia **(Fig. 6A)** and FRET experiments using the Raichu-RhoA biosensor (Yoshizaki et al., 2003) in living primary cortical microglia **(Fig. 6B)** showed that proinflammatory stimulation with LPS reduced RhoA activity compared with controls. Fast and robust reduction of RhoA activity was also observed in living CHME3 microglial cell line subjected to hypoxia **(Fig. 6C).** In contrast, exposure to the anti-inflammatory cytokine IL-4 substantialy increased RhoA activity in living CHME3 microglia **(Fig. 6D)**.

We then investigated whether reduction of RhoA activity was necessary for microglial activation. We co-transfected CHME3 microglia with a constitutively active RhoA mutant ($RhoA^{Q63L}$) and a ROS FRET biosensor (Guzy et al., 2005) to evaluate the production of ROS after challenging microglia with LPS or subjecting them to hypoxia. Our results showed that LPS or hypoxia-mediated ROS generation were largely attenuated in living microglia expressing $RhoA^{Q63L}$ **(Figs. 6E and F)**, suggesting that reduction of RhoA activity was necessary for microglia activation in those paradigms.

RhoB and RhoC do not compensate for the lack of RhoA in microglia

Given that RhoA, RhoB and RhoC share high degree of similarity (Wheeler and Ridley, 2004), we asked whether depleting RhoB or RhoC would also lead to microglial activation. Knocking down RhoB or RhoC expression using lentiviral-mediated shRNA delivery **(validation in Suppl. Figs. 7A and B)** did not lead to variations in ROS production **(Suppl. Fig. 7C)** or in glutamate release **(Suppl. Fig. 7D)** in living microglia. To check whether the proinflammatory polarization of microglia triggered by RhoA depletion could be explained by a compensatory RhoC upregulation, we measured the activation of RhoC by FRET in living microglia depleted of RhoA and detected no significant difference in basal RhoC activation **(Suppl. Fig. 7E)**. We also showed that RhoC activation was not altered in living microglia exposed to LPS or subjected to hypoxia **(Suppl. Fig. 7F)**.

Depletion of RhoA activates microglia by modulating Csk/Src signaling pathway

Csk, the endogenous repressor of the Src family of tyrosine kinases (SFKs) (Nada et al., 1991), is a protein tyrosine kinase that plays key roles in inflammation

(Thomas et al., 2004). Besides, Src, the prototype SFK member, is a modulator of the proinflammatory polarization of microglia (Socodato et al., 2015b). Therefore, we hypothesized that RhoA might control microglia homeostasis and activation through Csk/Src signaling.

To test this hypothesis, we first evaluated whether ablating RhoA in microglia affected Csk expression. To do that, we studied Csk transcript levels by qRT-PCR in FACS-sorted microglia from control and RhoA cKO brains. We observed a significant decrease of Csk mRNA transcripts in RhoA cKO microglia when compared to control microglia (**Fig 7A**). To evaluate wheter this decrease in Csk mRNA, also led to alterations in Csk protein amounts, we performed Western blot analysis on cell lysates obtained from RhoA KD N9 microglia and observed a decrease in Csk protein content compared with those of controls **(Fig 7B)**. In addition, double-labelling immunocytochemistry using antibodies against Csk and CD11b in RhoA KD rat primary cortical microglial cultures further confirmed that depleting RhoA resulted in a reduction of Csk expression **(Fig 7C).**

Because Csk is the endogenous repressor of Src, we next assessed whether RhoA depletion resulted in activation of Src. Double-labelling immunohistochemistry using antibodies against the active form of Src (phosphorylated on $pTyr^{416}$) and GFP (detecting $EYFP^{+}$ microglia) on brain sections from CT and RhoA cKO mice showed that RhoA cKO microglia had increased amouts of active Src relative to CT microglia (**Fig. 7D**). Furthermore, Western blot analysis of protein lysates obtained from RhoA KD N9 microglia showed an increase in Src $pTyr^{416}$ compared with those of controls **(Fig. 7E).** Using the KRas Src YPet biosensor (Ouyang et al., 2008) we then showed by FRET that the specific activity of Src increased in living CHME3 microglia depleted of RhoA **(Fig. 7F)**. We also revealed that exposing microglia to LPS or subjecting microglia to hypoxia

decreased Csk amounts (**Fig. 7G)** and induced the activation of Src (**Fig. 7H and I)**. Further confirming that RhoA in microglia controls Csk/Src pathway, expressing the constitutively active RhoA mutant $RhoA^{Q63L}$ significantly attenuated the decrease in Csk expression **(Fig. 7G)** and the increase in Src activation **(Fig. 7H and I)** triggered either by LPS or hypoxia. We concluded that in microglia, the Csk/Src pathway is under a RhoA inhibitory tonus and that RhoA depletion leads to Csk downregulation and consequent activation of Src.

Next, we studied whether microglial activation caused by RhoA depletion occurred through Src. Resembling the microglial activation profile after RhoA depletion (**Fig. 1 and Suppl. Fig. 2**), either the depletion of Csk with shRNA or the activation of Src by overexpressing the constitutively active Src mutant Src^{Y527F} in microglia induced NF-□B nuclear translocation and increased the release of TNF and glutamate (**Fig. 7J-L**). On the other hand, the expression of the dominant negative Src mutant Src^{Y416F} in RhoA KD N9 microglia reduced the activation of NF-kB, by showing significant less translocation of the GFP-tagged p65 subunit of NF-□B into the nucleus of these cells **(Suppl. Fig. 8A).** Consistent with this, we observed that expression of Src^{Y416F} resulted in lesser expression of iNOS **(Suppl. Fig. 8B)** and in reduced TNF release **(Suppl. Fig. 8C)** in RhoA KD N9 microglia compared with controls. Inhibition of Src with SKI-1 also decreased the phagocytic capacity of microglia depleted of RhoA (**Suppl. Fig. 8D**). Then, we transfected CHME3 microglia co-expressing the constitutively active $RhoA^{Q63L}$ mutant and the chemically-inducible Src heteromerization quimera (RapR-Src, (Karginov et al., 2010)) with the ROS (HSP probe) or with the glutamate release (FLIPE probe) FRET biosensor. Inducing fast Src activation by switching on RapR-Src with rapamycin led to robust ROS generation **(Suppl. Fig. 8E)** and glutamate release **(Suppl. Fig. 8F)** in living microglia. The fact that the expression of $RhoA^{Q63L}$ did not prevent ROS production

or glutamate release following RapR-Src activation suggested that Src tyrosine kinase activity was a downstream event in RhoA-mediated microglial dysregulation. This was further confirmed by showing that pharmacological inhibition of Src activation with SKI-1 in Csk KD N9 microglia prevented the nuclear translocation of the GFP-tagged p65-subunit of NF-kB **(Suppl. Fig. 8G)** and the release of TNF **(Suppl. Fig. 8H)** or glutamate **(Suppl. Fig. 8I)**. Collectively, these data suggest that the RhoA control of microglial activation occurs by downstream regulation of Csk/Src signaling pathway.

Src inhibition in RhoA cKO brains attenuates microglia deregulation, prevents synapse loss and restores cognition

After showing that RhoA depletion activates microglia through Src activation, we then hypothesized that blocking Src would rescue, to some extent, the deregulation of microglial homeostasis found in RhoA cKO brains. To do that, we injected RhoA cKO mice with tamoxifen and with AZD 0530, a clinically relevant Src inhibitor (Frail et al., 2015), and one month later (**Fig. 8A**), we analysed microglial numbers and gene expression in the brains of RhoA cKO mice. Results showed that Src inhibition abrogated the decrease in microglial cell numbres observed after microglial ablation of RhoA (**Fig. 8B**). Moreover, the decrease in the transcript levels of the microglia maintenance gene *csfr1* and of the microglia signature genes *p2ry12*, *mertk*, *gpr34*, and *pros1* were significantly attenuated in RhoA cKO brains treated with AZD 0530 (**Fig. 8C**). In addition, AZD 0530 significantly prevented the increase of mRNA transcript of the proinflammatory cytokines *tnf*, *il-1β* and *il-6* (**Fig. 8C**), the decrease of mRNA transcripts encoding the inflammation-related molecules *c1qC*, *c1qB*, *trem2*, *tlr7* and *tlr4* (**Fig. 8C**) and the reduction of mRNA transcript of the antioxidant-related genes *gclc*, *txnrd1* and *slc23a2* (**Fig. 8C**) in RhoA cKO brains.

Because microglia-specific ablation of RhoA led to their proinflammatory polarisation causing synaptic loss and deficits in recognition memory, we then evaluated synaptic markers and the performance in the NOR test of RhoA cKO mice injected with AZD 0530. We found that the protein amounts of the classical synaptic markers synaptophysin and PSD-95 in the hippocampus of mutant mice injected with AZD 0530 were significantly higher than in the hippocampus of mutant animals injected only with vehicle solution (**Fig. 8D**). We also found that mutant mice injected with AZD 0530 spent more time exploring the novel object (**Fig. 8E**) and discriminated the novel object more efficiently than RhoA cKO mice injected with vehicle solution (**Fig. 8F**). No differences in total object exploration time were observed between RhoA cKO animals injected with AZD or the vehicle (**Fig. 8G**), indicating that RhoA cKO under AZD 0530 performed substantially better in the NOR test.

Discussion

To define the mechanisms regulating microglia homeostasis in the adult brain under physiological conditions remains an important task that was greatly facilitated by the availability of microglia-specific Cre lines based on the insertion of a Cre^{ER} cassette into the Cx3cr1 locus (Goldmann et al., 2013; Parkhurst et al., 2013). Here, by crossing *Cx3cr1*$^{CreER\text{-}eYFP}$ mice (Parkhurst et al., 2013) with RhoA floxed mice (Herzog et al., 2011; Jackson et al., 2011) we studied for the first time the *bona fide* role(s) of RhoA in adult brain microglia under physiological conditions. This approach circumvented some of the limitations of previous studies of RhoA signaling using overexpression of RhoA dominant mutants (Bianchi et al., 2011; Moon et al., 2013; Ohsawa et al., 2000), which may trigger off-target and trans-dominant effects (Wang and Zheng, 2007; Zhou and Zheng, 2013), as well as the use of C3 exoenzyme toxin (Hoffmann et al., 2008; Rattan et al., 2003), which not only inhibits RhoA but also RhoB and RhoC (Chardin et al., 1989; Mohr et al., 1992).

Microglia-specific ablation of RhoA disrupted microglial homeostasis **(Fig. 9)** leading to their activation and neuroinflammation, which is a hallmark of several brain disorders (Perry and Holmes, 2014). Because the loss of RhoA reduced the numbers and expression of microglia maintenance and signature genes in the absence of BBB leakage and infiltrating peripheral monocytes or $CD4^+$ T cells, it is likely that self-renewing of resident $Cx3cr1^+$ microglia requires RhoA signaling. It is thought that autonomous self-renewing of the brain resident $Cx3cr1^+$ cell population occurs throughout the lifetime of organisms to maintain the stability of the microglia cell population (Bruttger et al., 2015; Elmore et al., 2014).

BBB breakdown is a common finding in neurological conditions (Palmer, 2010), but it is still not clear whether BBB breakdown is an initial event leading to neuronal

death or whether it is a consequence (Obermeier et al., 2013). Microglia-specific ablation of RhoA led to increased oxidative stress and expression of proinflammatory cytokines, known to increase BBB permeability (Rochfort and Cummins, 2015). However, the absence of vessel leakage and of infiltrating T-lymphocytes into the brain parenchyma of RhoA cKO mice suggested that the BBB was intact. In this particular, it is possible that the levels of ROS and inflammatory cytokines were not sufficient to trigger BBB leakage. Nevertheless, we observed pronounced cytoarchitecture changes and angiogenesis in RhoA cKO brains, likely to be caused by a combination of increased amounts of inflammatory cytokines, ROS generation, and glutamate release by microglia.

Inflammatory cytokines, ROS, and glutamate secretion by microglia can adversely impact neuronal viability (Brown and Neher, 2014). Conversely, microglia-triggered inflammation can induce neurons to expose phosphatidylserine on their cell surface and be “eaten” by microglia (Brown and Neher, 2014). In addition, genome-wide association studies indicate that mutations on phagocytosis-related genes might increase the risk for developing neurodegenerative diseases, suggesting that microglia phagocytosis of neurons likely contributes to the pathophysiology of brain disorders. Therefore, the increase of microglia phagocytic capacity together with microglia-induced inflammation could account for the decreased neuronal numbers found in the brains of RhoA cKO mice.

Ablation of RhoA in adult hippocampal microglia was sufficient to induce synaptic and neuronal loss, associated with deposits of hyperphosphorylated Tau, LTP impairment and cognitive deficits. Still, this did not affect the different forms of short-term synaptic plasticity, evidenced by PTP and PPF protocols, which is in line with the view that basal neurotrasmitter secretion does not contribute to steady state synaptic

assembly (Varoqueaux et al., 2002; Verhage et al., 2000). Another possibility is that homeostatic synaptic scaling (Turrigiano et al., 1998) at the postsynaptic terminal largely compensated the decrease of both synapse and neuronal numbers (Turrigiano, 2007), preserving short-term plasticity in the RhoA cKO hippocampus. Collectively, microglia activation in RhoA cKO largely influenced the hippocampal synaptic landscape, which is important for long-term synaptic plasticity (Scannevin and Huganir, 2000). It is likely that synaptic loss together with the decreased neuronal numbers were responsible for LTP alterations and the deficits in recognition memory observed in RhoA cKO animals. In line with our findings, similar changes in synapse and neuronal numbers, LTP and cognition are also observed in animal models for neurodegenerative disorders, including Alzheimer´s disease (Trinchese et al., 2004; Zhang et al., 2012), supporting the hypothesis that chronic loss of RhoA specifically in microglia initiates a degenerative pathology in the adult brain.

Our data demonstrate that not only loss of RhoA in microglia caused their proinflammatory activation, but also that proinflammatory activation triggered by LPS or hypoxia required decrease of RhoA activity. These observations contrast with those made in other cell types, including monocytes, in which LPS treatment induces RhoA activity, and subsequent activation of NF-κB to trigger inflammation (Chen et al., 2002), thereby suggesting that modulation of RhoA activity can have different functional effects in monocytes/macrophages and microglia. Accordingly, conditional-gene targeting studies show that many of the specific pathways regulated by a given RhoGTPase are cell type and stimulus specific, and that knowing the role of a RhoGTPase in a given cell type cannot necessarily predict its function and signaling mechanisms in another one (Pedersen and Brakebusch, 2012; Wang and Zheng, 2007).

RhoA executes its functions through multiple pathways and effectors, and it is to

be expected that the loss of RhoA might disturb the functions and/or interactions of more than one of its effectors. In line with this, knocking out RhoA or knocking out one of its effectors can give rise to discordant phenotypes. For instance, knocking out RhoA in the mouse spinal cord neuroepithelium does not cause cytokinesis defects (Herzog et al., 2011), whereas knocking out the RhoA effector citron-kinase leads to impaired cytokinesis (Di Cunto et al., 2000). This could also explain why specific loss of RhoA in microglia disrupted their homeostasis whereas the pharmacological inhibition of the RhoA effector ROCK attenuates neuroinflammation in different neurological conditions (Chen et al., 2013; Mueller et al., 2005). Another factor potentially contributing for the disparity of these 2 phenotypes is that in addition to being activated by RhoA, ROCK can also be regulated by RhoE/Rnd3 (Riento et al., 2003) or by RhoC (Riento and Ridley, 2003). Our data, however, suggest that RhoC does not play a significant role in microglia proinflammatory activation. Moreover, certain care must be exerted when interpreting results obtained with ROCK inhibitors (for intance Y27632 or fasudil), as these kinase inhibitors in addition to inhibiting ROCK also inhibit protein kinase C (PKC) and other kinases involved in cytoskeleton regulation (Vigil and Der, 2013) that might potentially modulate microglial function. In this particular, PKC activation is important for TLR-mediated inflammation (Loegering and Lennartz, 2011) and its inhibition reduces microglial activation (Kim et al., 2005; Wen et al., 2011).

RhoA controlled microglia homeostasis and activation by restraining downstream Src signaling (**Fig. 9A**). The depletion of RhoA in microglia decreased Csk mRNA and consequently protein amounts, which led to increased Src phosphorylation and activation. Increased microglia activation and phagocytosis, upon RhoA depletion, was significantly inhibited by blockade of Src. In vivo, inhibition of Src activity in RhoA cKO mice, using the clinically relevant Src inhibitor AZD 0530 (Frail et al., 2015), substantially restored microglial cell numbers, the expression levels of microglia

signature transcripts, and the levels of gene transcripts involved in immune regulation and anti-oxidant responses. In addition, RhoA cKO mice injected with AZD 0530 displayed higher amounts of synaptic proteins and performed substantially better in the NOR test compared with RhoA cKO mice injected with vehicle solution, indicating that modulating Src activity might have therapeutic value to prevent or attenuate behavioural deficits associated with microglial dysfunction.

Microglia-specific ablation of RhoA in the adult brain resulted in their sustained deregulation, which culminated in a neurodegenerative pathology (**Fig. 9B**). We also found that depletion of RhoA resulted in microglia activation and phagocytosis through downstream activation of the Csk/Src pathway. Of note, loss of RhoA in microglia leads to phenotypic changes (neuroinflammation, astroglosis, agiogenesis, long-term synaptic plasticity impairment, memory deficits with synapse and neuronal loss) that are also commonly observed in neurodegenerative disorders. In this regard, our data provide additional support to the emergent notion of “microgliopathy” (Prinz and Priller, 2014), in which microglia dysfunction, by itself, can be primary cause of brain disease.

Experimental Procedures

Microglia RhoA-deficient mice: All mice experimests were approved by Direção-Geral de Alimentação e Veterinária (DGAV). Cx3cr1^{CreER} mice were purchased from Jackson Laboratories. In such mice, the *Cx3cr1* promoter drives CreER expression specifically in microglia (Parkhurst et al., 2013). Mice homozygous for the *RhoA* floxed allele (Herzog et al., 2011; Jackson et al., 2011) were backcrossed at least for 10 generations and were kept at the I3S animal facility. All genotypes were determined by PCR on genomic DNA. Primers used for RhoA floxed alleles were fw: AGC CAG CCT CTT GAC CGA TTT A; rv = TGT GGG ATA CCG TTT GAG CAT. Primers for CreER insertion were fw: AAGACTCACGTGGACCTGCT; wt rv: AGGATGTTGACTTCCGAGTG; mutant rv: CGGTTATTCAACTTGCACCA. RhoA floxed mice were crossed with Cx3cr1^{CreER} mice. Progeny of interest were: Control (RhoA$^{fl/wt}$:Cx3cr1^{CreER+} or RhoA$^{fl/fl}$) and RhoA cKO (RhoA$^{fl/fl}$:Cx3cr1^{CreER+}). Mice were given tamoxifen (10 mg *per* animal by oral gavage) at P26 and P28 and then analyzed at P65-80. All experiments were performed on mice kept on a C57Bl/6 background with no sex difference for statistical pooling. The only exception was in the electrophysiological recordings and in behavioral tests where only male CT and RhoA cKO mice were used.

Flow cytometry and cell sorting: For characterization of microglia and macrophages in the samples, the following markers were used: CD45-PE (BioLegend 103106), CD11b-Alexa647 (BioLegend 101218) and Ly6C-PerCP/Cy5.5 (BioLegend 128012). Microglial and macrophages were collected from the tissues (brain, blood, spleen and liver) of CT and RhoA cKO mice using density gradient separation. In brief, mice were anesthetized and then perfused with ice-cold PBS. For single cell suspensions, tissues were quickly dissected, placed on ice-cold RPMI and mechanically homogenized. Cell suspension

was passed through a 100µM cell strainer and centrifuged over a discontinuous 70%/30% Percoll gradient. Cells on the interface were collected, pelleted, washed extensively and then resuspended in FACS buffer before antibody staining for 30 min at 4 °C in the dark. Compensation settings were determined using spleen from both CT and RhoA cKO. Cell suspensions were evaluated on a FACS Canto II analyser (BD Immunocytometry Systems). Cell sorting was performed on a FACS ARIA cell sorter. Data were analyzed by FlowJo X10 software (TreeStar).

FRET-based live cell imaging and biosensor quantification: Microglial cells were plated on plastic-bottom culture dishes (µ-Dish 35 mm, iBidi). Imaging was performed using a Leica DMI6000B inverted microscope. The excitation light source was a mercury metal halide bulb integrated with an EL6000 light attenuator. High-speed low vibration external filter wheels (equipped with CFP/YFP excitation and emission filters) were mounted on the microscope (Fast Filter Wheels, Leica Microsystems). A 440-520nm dichroic mirror (CG1, Leica Microsystems) and a PlanApo 63X 1.3NA glycerol immersion objective were used for CFP and FRET images. Images were acquired with 4x4 binning using a digital CMOS camera (ORCA-Flash4.0 V2, Hamamatsu Photonics). Shading illumination was online-corrected for CFP and FRET channels using a shading correction routine implemented for the LAS AF software. At each time-point, CFP and FRET images were sequentially acquired using different filter combination (CFP excitation plus CFP emission, and CFP excitation plus YFP emission, respectively).

Quantification of FRET biosensores were performed as before (Portugal et al., 2017; Socodato et al., 2015a; Socodato et al., 2015b). In brief, images were exported as 16-bit tiff files and processed in FIJI software. Background was dynamically subtracted from all frames from both channels and images were filtered using a Kalman stack filter. Segmentation was achieved on a pixel-by-pixel basis using a modification of the

Phansalkar algorithm. After background subtraction and thresholding, binary masks were generated for the CFP and FRET images. Original CFP and FRET images were masked, registered and bleach-corrected. Ratiometric images (CFP/FRET for KRas Src YPet probe, HSP33 ROS probe and FLIPE glutamate release probe or FRET/CFP for Raichu-RhoA and Flare.RhoC sensors) were generated as 32-bit float-point tiff images. Values corresponding to the mean gray values were generated using the multi calculation function in FIJI and exported as mentioned above.

Quantitative RT-PCR: qRT-PCR was carried out using iQ™ SYBR® Green Supermix on an iQ™5 multicolor real-time PCR detection system (Bio-Rad). The efficiency was analyzed using a log-based standard curve. Expression of PCR transcripts between genotypes was calculated using the $2^{-\Delta Ct}$ method with *Yhwaz* serving as the internal control gene.

Electrophysiology:

Preparation of acute hippocampal slices. For electrophysiological recordings, acute hippocampal slices from P65-80 male control ($RhoA^{fl/fl}$) and RhoA cKO ($RhoA^{fl/fl}$:$Cx3cr1^{CreER+}$) mice were prepared. All procedures were carried out according to the European Union Guidelines for Animal Care (European Union Council Directive 2010/63/EU) and Portuguese law (DL 113/2013) with the approval of the Institutional Animal Care and Use Committee.

Animals were sacrificed by decapitation after cervical displacement and the brain was rapidly removed in order to isolate the hippocampus. Hippocampi were dissected in ice-cold artificial cerebrospinal fluid (aCSF) containing (in mM): 124 NaCl, 3 KCl, 1.2 NaH_2PO_4, 25 $NaHCO_3$, 2 $CaCl_2$, 1 $MgSO_4$ and 10 glucose), which was continuously gassed with 95%O2/5% CO2. Hippocampal slices were quickly cut perpendicularly to

the long axis of the hippocampus (400 µm thick) with a McIlwain tissue chopper and allowed to recover functionally and energetically for at least 1 h in a resting chamber filled with continuously oxygenated aCSF, at room temperature (22–25°C), before being set up for electrophysiological recordings.

Extracellular recordings of fEPSPs. Following the recovery period, slices were transferred to a recording chamber for submerged slices (1 ml capacity plus 5 ml dead volume) and were constantly superfused at a flow rate of 3 ml/mim with aCSF kept at 32ºC, gassed with 95% O_2 – 5%CO_2. Evoked fEPSP were recorded extracellularly using a microelectrode (4 to 8 MΩ resistance) filled with aCSF solution placed in the *stratum radiatum* of the CA1 area. fEPSP data were acquired using an Axoclamp-2B amplifier (Axon Instrumnets, Foster City, CA). fEPSPs were evoked by stimulation through a concentric electrode to the Schaffer collateral fibres. Each individual stimulus consisted of a 0.1 ms rectangular pulse applied once every 20s, except otherwise indicated. Averages of six consecutive responses were continuously acquired, digitized with the WinLTP program (Anderson and Collingridge, 2001) and quantified as the slope of the initial phase of the averaged fEPSPs (and the amplitude of presynaptic fibre voley while performing input/output analysis). The stimulus intensity was adjusted at the beginning of the experiment to obtain a fEPSP slope close to 1 mV/ms, which corresponded to about 50% of the maximal fEPSP slope.

For input/output curves (I/O), after obtaining a stable baseline under the standard stimulation conditions, the stimulus intensity was increased by 20 µA every 4 min (60-320 µA). The I/O curves were plotted as the fEPSP slope against the stimulus intensity, as the presynaptic fiber volley (PSFV) amplitude against stimulus intensity, and as the fEPSP slope against PSFV amplitude, which provides a measure of synaptic efficiency.

The max slope values were obtained by extrapolation upon nonlinear fitting of the I/O curve, an F-test being used to determine differences between the parameters.

Paired-pulse facilitation (PPF) was quantified as the ratio between the slopes of two consecutive fEPSPs (fEPSP1/fEPSP0) elicited with 50 ms interstimulus interval, each pair being delivered once every 15 sec. Six paired-pulse responses were averaged to obtain a PPF value on each slice.

θ-burst stimulation was used to induce LTP because this pattern of stimulation is considered closer to what physiologically occurs in the hippocampus during episodes of learning and memory in living animals (Albensi et al., 2007). After obtaining a stable recording of the fEPSP slope, a θ-burst of stimuli, consisting of 1 train of 4 bursts (200 ms interburst interval), each burst being composed of 4 pulses delivered at 100 Hz [1 x (4 x 4)], was applied, and the stimulus paradigm was then resumed to pre-burst conditions up to the end of the recording period (60 min after burst stimulation). LTP magnitude was quantified as % change in the average slope of the fEPSP taken from 50-60 minutes after LTP induction as compared with the average slope of the fEPSP measured during the 10 min before induction of LTP. Posttetanic potentiation (PTP) was assessed as the average fEPSP slope obtained in the first 8 min after LTP induction (Habets and Borst, 2007).

Because each slice allows recordings from two independent pathways, the usual protocol was to record first PPF data by stimulation of one pathway, then I/O data by stimulating the second pathway, then PTP and LTP data by delivering stimulation again in the first. In any case, fEPSPs were recorded under basal stimulation conditions (standard stimulus intensity and frequency) and stability of fEPSP slope values guaranteed for more than 10 min before changing any protocol parameter. One or two slices per animal were tested at each experimental day.

Behavioral tests: All testing procedures were conducted in the dark phase of the light/dark cycle. Before each session, mice were removed from their home cage in the colony room and brought into the adjacent testing rooms (illuminated with 100 lux and attenuated noise). Behavioural test were performed in the following order: (1) elevated plus-maze; (2) open field; (3) novel object recognition. All tests were video-recorded. In the elevated plus-maze and open-field tests movement and location of mice were analyzed by an automated tracking system equipped with an infrared-sensitive camera (Smart Video Tracking Software v 2.5, Panlab, Harvard Apparatus). Data from the object recognition test were analyzed using the Observer 5 software (Noldus Information Technology, Wageningen, The Netherlands). All apparatus were thoroughly cleaned with neutral soap after each test session.

Elevated plus-maze (EPM): The maze was made of opaque grey PVC consisting of four arms arranged in a plus-shaped format; two arms have surrounding walls (closed arms, 37x6 cm x18 cm-high), while the two opposing arms have no walls (open arms, 37x6 cm). The apparatus is elevated by 50 cm above the ground. Mice were placed on the central platform facing an open arm and were allowed to explore the maze for 5 minutes. Open arms entries and time spent in open arms were obtained automatically (video tracking) and used to assess anxiety-like behavior.

Open field (OF): Mice were placed in the center of an OF apparatus (40 x 40 x 40 cm) and then allowed to move freely for 10 min. The distance travelled, peripheral activity and center activity (locomotion in the central section of the OF) were obtained automatically (video tracking).

Novel object recognition (NOR): The NOR test was performed as previously described (Leger et al., 2013). Briefly, the test apparatus consists of an open box and the objects used are made of plastic, glass or metal in three different shapes: cubes, pyramids and cylinders. The test consists of three phases. During habituation phase mice are allowed to explore the apparatus for 10 min (time used to perform OF test). The following day, the acquisition/sample phase starts by placing each mouse in the apparatus with two identical objects (familiar) for 10min. Then the mouse goes back to its home cage. After 4 hours (inter-trial interval, ITI), the retention/choice session is performed. In this phase, the apparatus contains a novel object and a copy of the previous familiar object, animals are allowed to explore these objects for 3 min. The time spent exploring the novel object serves as the measure of recognition memory for the familiar object. Exploration was defined as follows: mouse touched the object with its nose or the mouse's nose was directed toward the object at a distance shorter than 2 cm (Ennaceur et al., 2005). Circling or sitting on the object was not considered exploratory behavior. The difference between the exploration time for novel and familiar objects was used as indicator of object recognition: a) if > 0, there is apreference for the new object; b) if = 0, null preference; c) if < 0, there is a preference for the familiar object (Ennaceur et al., 2005). The index of discrimination (DI) was calculated as index of memory function, DI = (time exploring the novel object) / (total time spent exploring both objects).

Statistics: A 95% confidence interval was used for statistical evaluation and $p < 0.05$ was considered statistically significant difference in all sampled groups. Experimental units in individual replicates were prior evaluated for Gaussian distribution using the D'Agostino & Pearson omnibus normality test with GraphPad Prism. When comparing only 2 experimental groups Mann-Whitney test for data with non-normal distribution or unpaired Student t test with equal variance assumption for data with normal distribution

was used. When comparing 3 or more groups with data without normal distribution the Kruskal-Wallis test followed by Dunn`s multiple comparation was used and One-way ANOVA followed by the Bonferroni multiple comparation test was used for data with normal distribution. Comparison between mice genotypes in brain histological sections were performed using paired Student t test. Two-way ANOVA was used to determine significative differences between genotypes in the Sholl analysis of microglia in the brain. All statistical analyses were carried out using the Graph Pad Prism 6.0 software.

To minimize bias, experimental groups using cultured cells were assigned using simple random sampling. All imaging quantifications (cell cultures or mice tissue sections) were performed blinded. Besides, a rotational scheme was employed between researchers for acquiring and quantifying the imaging sets where a given researcher never quantified the same imaging set he/she acquired.

Further methodological details are available in the supplemental information (SI) section.

Acknowledgements

FEDER and FCT, Portugal (Norte-01-0145-FEDER-000008000008—Porto Neurosciences and Neurologic Disease Research Initiative at I3S, supported by Norte Portugal Regional Operational Programme (NORTE 2020), under the PORTUGAL 2020 Partnership Agreement, through the European Regional Development Fund (ERDF); FCOMP-01-0124-FEDER-021333) supported work in JBR lab. FEDER, FCT and AIBILI, Portugal (PTDC/NEU-OSD/1113/2012 and Strategic Projects PEst-C/SAU/UI3282/2011-2013, UID/NEU/04539/2013) supported work in AFA lab. RPC is a research fellow from CNPq and Faperj (Brazil). RLA is supported by an FCT grant (PD/BD/114266/2016). AM was supported by FCT (IF/00753/2014 and CP1244/CT0005). TS was supported by FCT (IF/00875/2012). RS, CCP, FIB and SHV hold postdoctoral fellowships from FCT (Refs: SFRH/BPD/91833/2012, FRH/BPD/91962/2012, SFRH/BPD/86830/2012 and (SFRH/BPD/ 81627/2011), respectively).

Authors declare no conflict of interest.

References

abd-el-Basset, E., and S. Fedoroff. 1995. Effect of bacterial wall lipopolysaccharide (LPS) on morphology, motility, and cytoskeletal organization of microglia in cultures. *Journal of neuroscience research*. 41:222-237.

Albensi, B.C., D.R. Oliver, J. Toupin, and G. Odero. 2007. Electrical stimulation protocols for hippocampal synaptic plasticity and neuronal hyper-excitability: are they effective or relevant? *Experimental neurology*. 204:1-13.

Anderson, W.W., and G.L. Collingridge. 2001. The LTP Program: a data acquisition program for on-line analysis of long-term potentiation and other synaptic events. *Journal of neuroscience methods*. 108:71-83.

Bianchi, R., E. Kastrisianaki, I. Giambanco, and R. Donato. 2011. S100B protein stimulates microglia migration via RAGE-dependent up-regulation of chemokine expression and release. *The Journal of biological chemistry*. 286:7214-7226.

Block, M.L., L. Zecca, and J.S. Hong. 2007. Microglia-mediated neurotoxicity: uncovering the molecular mechanisms. *Nature reviews. Neuroscience*. 8:57-69.

Brown, G., and J. Neher. 2014. Microglial phagocytosis of live neurons. *Nature reviews. Neuroscience*. 15:209.

Bruttger, J., K. Karram, S. Wortge, T. Regen, F. Marini, N. Hoppmann, M. Klein, T. Blank, S. Yona, Y. Wolf, M. Mack, E. Pinteaux, W. Muller, F. Zipp, H. Binder, T. Bopp, M. Prinz, S. Jung, and A. Waisman. 2015. Genetic Cell Ablation Reveals Clusters of Local Self-Renewing Microglia in the Mammalian Central Nervous System. *Immunity*. 43:92-106.

Bustelo, X.R., V. Sauzeau, and I.M. Berenjeno. 2007. GTP-binding proteins of the Rho/Rac family: regulation, effectors and functions in vivo. *BioEssays : news and reviews in molecular, cellular and developmental biology*. 29:356-370.

Butovsky, O., M.P. Jedrychowski, C.S. Moore, R. Cialic, A.J. Lanser, G. Gabriely, T. Koeglsperger, B. Dake, P.M. Wu, C.E. Doykan, Z. Fanek, L. Liu, Z. Chen, J.D. Rothstein, R.M. Ransohoff, S.P. Gygi, J.P. Antel, and H.L. Weiner. 2014. Identification of a unique TGF-beta-dependent molecular and functional signature in microglia. *Nature neuroscience*. 17:131-143.

Cappello, S., C.R. Bohringer, M. Bergami, K.K. Conzelmann, A. Ghanem, G.S. Tomassy, P. Arlotta, M. Mainardi, M. Allegra, M. Caleo, J. van Hengel, C. Brakebusch, and M. Gotz. 2012. A radial glia-specific role of RhoA in double cortex formation. *Neuron*. 73:911-924.

Chardin, P., P. Boquet, P. Madaule, M.R. Popoff, E.J. Rubin, and D.M. Gill. 1989. The mammalian G protein rhoC is ADP-ribosylated by Clostridium botulinum exoenzyme C3 and affects actin microfilaments in Vero cells. *The EMBO journal*. 8:1087-1092.

Chen, L.Y., B.L. Zuraw, F.T. Liu, S. Huang, and Z.K. Pan. 2002. IL-1 receptor-associated kinase and low molecular weight GTPase RhoA signal molecules are required for bacterial lipopolysaccharide-induced cytokine gene transcription. *Journal of immunology (Baltimore, Md. : 1950)*. 169:3934-3939.

Chen, M., A. Liu, Y. Ouyang, Y. Huang, X. Chao, and R. Pi. 2013. Fasudil and its analogs: a new powerful weapon in the long war against central nervous system disorders? *Expert opinion on investigational drugs*. 22:537-550.

Chong, C.M., N. Ai, and S.M. Lee. 2016. ROCK in CNS: different roles of isoforms, and therapeutic target for neurodegenerative disorders. *Current drug targets*.

Crotti, A., and R.M. Ransohoff. 2016. Microglial Physiology and Pathophysiology: Insights from Genome-wide Transcriptional Profiling. *Immunity*. 44:505-515.

Daulatzai, M.A. 2016. Fundamental role of pan-inflammation and oxidative-nitrosative pathways in neuropathogenesis of Alzheimer's disease in focal cerebral ischemic rats. *American journal of neurodegenerative disease*. 5:102-130.

DeGeer, J., and N. Lamarche-Vane. 2013. Rho GTPases in neurodegeneration diseases. *Experimental cell research*. 319:2384-2394.

Dheen, S.T., C. Kaur, and E.A. Ling. 2007. Microglial activation and its implications in the brain diseases. *Curr Med Chem*. 14:1189-1197.

Di Cunto, F., S. Imarisio, E. Hirsch, V. Broccoli, A. Bulfone, A. Migheli, C. Atzori, E. Turco, R. Triolo, G.P. Dotto, L. Silengo, and F. Altruda. 2000. Defective neurogenesis in citron kinase knockout mice by altered cytokinesis and massive apoptosis. *Neuron*. 28:115-127.

Di Filippo, M., P. Sarchielli, B. Picconi, and P. Calabresi. 2008. Neuroinflammation and synaptic plasticity: theoretical basis for a novel, immune-centred, therapeutic approach to neurological disorders. *Trends in pharmacological sciences*. 29:402-412.

Droppelmann, C.A., D. Campos-Melo, K. Volkening, and M.J. Strong. 2014. The emerging role of guanine nucleotide exchange factors in ALS and other neurodegenerative diseases. *Frontiers in cellular neuroscience*. 8:282.

Elmore, M.R., A.R. Najafi, M.A. Koike, N.N. Dagher, E.E. Spangenberg, R.A. Rice, M. Kitazawa, B. Matusow, H. Nguyen, B.L. West, and K.N. Green. 2014. Colony-stimulating factor 1 receptor signaling is necessary for microglia viability, unmasking a microglia progenitor cell in the adult brain. *Neuron*. 82:380-397.

Ennaceur, A., S. Michalikova, A. Bradford, and S. Ahmed. 2005. Detailed analysis of the behavior of Lister and Wistar rats in anxiety, object recognition and object location tasks. *Behavioural brain research*. 159:247-266.

Frail, D.E., M. Brady, K.J. Escott, A. Holt, H.J. Sanganee, M.N. Pangalos, C. Watkins, and C.D. Wegner. 2015. Pioneering government-sponsored drug repositioning collaborations: progress and learning. *Nature reviews. Drug discovery*. 14:833-841.

Gendron, T.F., and L. Petrucelli. 2009. The role of tau in neurodegeneration. *Molecular Neurodegeneration*. 4:13.

Ginhoux, F., M. Greter, M. Leboeuf, S. Nandi, P. See, S. Gokhan, M.F. Mehler, S.J. Conway, L.G. Ng, E.R. Stanley, I.M. Samokhvalov, and M. Merad. 2010. Fate mapping analysis reveals that adult microglia derive from primitive macrophages. *Science*. 330:841-845.

Ginhoux, F., and M. Guilliams. 2016. Tissue-Resident Macrophage Ontogeny and Homeostasis. *Immunity*. 44:439-449.

Goldmann, T., P. Wieghofer, P.F. Muller, Y. Wolf, D. Varol, S. Yona, S.M. Brendecke, K. Kierdorf, O. Staszewski, M. Datta, T. Luedde, M. Heikenwalder, S. Jung, and M. Prinz. 2013. A new type of microglia gene targeting shows TAK1 to be pivotal in CNS autoimmune inflammation. *Nature neuroscience*. 16:1618-1626.

Gomez-Nicola, D., N.L. Fransen, S. Suzzi, and V.H. Perry. 2013. Regulation of microglial proliferation during chronic neurodegeneration. *The Journal of neuroscience : the official journal of the Society for Neuroscience*. 33:2481-2493.

Gomez-Nicola, D., and V.H. Perry. 2015. Microglial dynamics and role in the healthy and diseased brain: a paradigm of functional plasticity. *The Neuroscientist : a review journal bringing neurobiology, neurology and psychiatry*. 21:169-184.

Govek, E.E., S.E. Newey, and L. Van Aelst. 2005. The role of the Rho GTPases in neuronal development. *Genes & development*. 19:1-49.

Greter, M., I. Lelios, and A.L. Croxford. 2015. Microglia Versus Myeloid Cell Nomenclature during Brain Inflammation. *Frontiers in immunology*. 6:249.

Guzy, R.D., B. Hoyos, E. Robin, H. Chen, L. Liu, K.D. Mansfield, M.C. Simon, U. Hammerling, and P.T. Schumacker. 2005. Mitochondrial complex III is required for hypoxia-induced ROS production and cellular oxygen sensing. *Cell metabolism*. 1:401-408.

Habets, R.L., and J.G. Borst. 2007. Dynamics of the readily releasable pool during post-tetanic potentiation in the rat calyx of Held synapse. *The Journal of physiology*. 581:467-478.

Healy, L.M., G. Perron, S.Y. Won, M.A. Michell-Robinson, A. Rezk, S.K. Ludwin, C.S. Moore, J.A. Hall, A. Bar-Or, and J.P. Antel. 2016. MerTK Is a Functional Regulator of Myelin Phagocytosis by Human Myeloid Cells. *Journal of immunology (Baltimore, Md. : 1950)*. 196:3375-3384.

Herzog, D., P. Loetscher, J. van Hengel, S. Knusel, C. Brakebusch, V. Taylor, U. Suter, and J.B. Relvas. 2011. The small GTPase RhoA is required to maintain spinal cord neuroepithelium organization and the neural stem cell pool. *The Journal of neuroscience : the official journal of the Society for Neuroscience*. 31:5120-5130.

Hodge, R.G., and A.J. Ridley. 2016. Regulating Rho GTPases and their regulators. *Nature reviews. Molecular cell biology*. 17:496-510.

Hoffmann, A., F. Hofmann, I. Just, S. Lehnardt, U.K. Hanisch, W. Brück, H. Kettenmann, G. Ahnert-Hilger, and M. Höltje. 2008. Inhibition of Rho-dependent pathways by Clostridium botulinum C3 protein induces a proinflammatory profile in microglia. *Glia*. 56:1162-1175.

Inoue, T., W.D. Heo, J.S. Grimley, T.J. Wandless, and T. Meyer. 2005. An inducible translocation strategy to rapidly activate and inhibit small GTPase signaling pathways. *Nature methods*. 2:415-418.

Jackson, B., K. Peyrollier, E. Pedersen, A. Basse, R. Karlsson, Z. Wang, T. Lefever, A.M. Ochsenbein, G. Schmidt, K. Aktories, A. Stanley, F. Quondamatteo, M. Ladwein, K. Rottner, J. van Hengel, and C. Brakebusch. 2011. RhoA is dispensable for skin development, but crucial for contraction and directed migration of keratinocytes. *Molecular biology of the cell*. 22:593-605.

Julian, L., and M.F. Olson. 2014. Rho-associated coiled-coil containing kinases (ROCK): structure, regulation, and functions. *Small GTPases*. 5:e29846.

Jung, S., J. Aliberti, P. Graemmel, M.J. Sunshine, G.W. Kreutzberg, A. Sher, and D.R. Littman. 2000. Analysis of fractalkine receptor CX(3)CR1 function by targeted deletion and green fluorescent protein reporter gene insertion. *Molecular and cellular biology*. 20:4106-4114.

Karginov, A.V., F. Ding, P. Kota, N.V. Dokholyan, and K.M. Hahn. 2010. Engineered allosteric activation of kinases in living cells. *Nature biotechnology*. 28:743-747.

Katayama, K., J. Melendez, J.M. Baumann, J.R. Leslie, B.K. Chauhan, N. Nemkul, R.A. Lang, C.Y. Kuan, Y. Zheng, and Y. Yoshida. 2011. Loss of RhoA in neural progenitor cells causes the disruption of adherens junctions and hyperproliferation. *Proceedings of the National Academy of Sciences of the United States of America*. 108:7607-7612.

Kaur, C. 1997. Effects of colchicine on amoeboid microglial cells in the postnatal rat brain. *Archives of histology and cytology*. 60:453-462.

Kim, D.C., S.H. Kim, M.W. Jeong, N.I. Baek, and K.T. Kim. 2005. Effect of rottlerin, a PKC-delta inhibitor, on TLR-4-dependent activation of murine microglia. *Biochemical and biophysical research communications*. 337:110-115.

Lawrence, T. 2009. The nuclear factor NF-kappaB pathway in inflammation. *Cold Spring Harbor perspectives in biology*. 1:a001651.

Leger, M., A. Quiedeville, V. Bouet, B. Haelewyn, M. Boulouard, P. Schumann-Bard, and T. Freret. 2013. Object recognition test in mice. *Nature protocols*. 8:2531-2537.

Loegering, D.J., and M.R. Lennartz. 2011. Protein kinase C and toll-like receptor signaling. *Enzyme research*. 2011:537821.

Mohr, C., G. Koch, I. Just, and K. Aktories. 1992. ADP-ribosylation by Clostridium botulinum C3 exoenzyme increases steady-state GTPase activities of recombinant rhoA and rhoB proteins. *FEBS letters*. 297:95-99.

Moon, M.Y., H.J. Kim, Y. Li, J.G. Kim, Y.J. Jeon, H.Y. Won, J.S. Kim, H.Y. Kwon, I.G. Choi, E. Ro, E.H. Joe, M. Choe, H.J. Kwon, H.C. Kim, Y.S. Kim, and J.B. Park. 2013. Involvement of small GTPase RhoA in the regulation of superoxide production in BV2 cells in response to fibrillar Abeta peptides. *Cellular signalling*. 25:1861-1869.

Mueller, B.K., H. Mack, and N. Teusch. 2005. Rho kinase, a promising drug target for neurological disorders. *Nature reviews. Drug discovery*. 4:387-398.

Nada, S., M. Okada, A. MacAuley, J.A. Cooper, and H. Nakagawa. 1991. Cloning of a complementary DNA for a protein-tyrosine kinase that specifically phosphorylates a negative regulatory site of p60c-src. *Nature*. 351:69-72.

Obermeier, B., R. Daneman, and R.M. Ransohoff. 2013. Development, maintenance and disruption of the blood-brain barrier. *Nature medicine*. 19:1584-1596.

Ohsawa, K., Y. Imai, H. Kanazawa, Y. Sasaki, and S. Kohsaka. 2000. Involvement of Iba1 in membrane ruffling and phagocytosis of macrophages/microglia. *Journal of cell science*. 113 (Pt 17):3073-3084.

Ouyang, M., J. Sun, S. Chien, and Y. Wang. 2008. Determination of hierarchical relationship of Src and Rac at subcellular locations with FRET biosensors. *Proceedings of the National Academy of Sciences of the United States of America*. 105:14353-14358.

Palmer, A.M. 2010. The role of the blood-CNS barrier in CNS disorders and their treatment. *Neurobiology of disease*. 37:3-12.

Parkhurst, C.N., G. Yang, I. Ninan, J.N. Savas, J.R. Yates, 3rd, J.J. Lafaille, B.L. Hempstead, D.R. Littman, and W.B. Gan. 2013. Microglia promote learning-dependent synapse formation through brain-derived neurotrophic factor. *Cell*. 155:1596-1609.

Pedersen, E., and C. Brakebusch. 2012. Rho GTPase function in development: how in vivo models change our view. *Experimental cell research*. 318:1779-1787.

Perry, V.H., and C. Holmes. 2014. Microglial priming in neurodegenerative disease. *Nature reviews. Neurology*. 10:217-224.

Portugal, C.C., R. Socodato, T. Canedo, C.M. Silva, T. Martins, V.S. Coreixas, E.C. Loiola, B. Gess, D. Rohr, A.R. Santiago, P. Young, R.D. Minshall, R. Paes-de-Carvalho, A.F. Ambrosio, and J.B. Relvas. 2017. Caveolin-1-mediated internalization of the vitamin C transporter SVCT2 in microglia triggers an inflammatory phenotype. *Science signaling*. 10.

Preissler, J., A. Grosche, V. Lede, D. Le Duc, K. Krugel, V. Matyash, F. Szulzewsky, S. Kallendrusch, K. Immig, H. Kettenmann, I. Bechmann, T. Schoneberg, and A. Schulz. 2015. Altered microglial phagocytosis in GPR34-deficient mice. *Glia*. 63:206-215.

Prinz, M., and J. Priller. 2014. Microglia and brain macrophages in the molecular age: from origin to neuropsychiatric disease. *Nature reviews. Neuroscience*. 15:300-312.

Rattan, R., S. Giri, A.K. Singh, and I. Singh. 2003. Rho a negatively regulates cytokine-mediated inducible nitric oxide synthase expression in brain-derived transformed cell lines: negative regulation of IKK α. *Free Radical Biology and Medicine*. 35:1037-1050.

Rice, R.A., E.E. Spangenberg, H. Yamate-Morgan, R.J. Lee, R.P. Arora, and M.X. Hernandez. 2015. Elimination of Microglia Improves Functional Outcomes Following Extensive Neuronal Loss in the Hippocampus. 35:9977-9989.

Ridley, A.J. 2015. Rho GTPase signalling in cell migration. *Current opinion in cell biology*. 36:103-112.

Riento, K., R.M. Guasch, R. Garg, B. Jin, and A.J. Ridley. 2003. RhoE binds to ROCK I and inhibits downstream signaling. *Molecular and cellular biology*. 23:4219-4229.

Riento, K., and A.J. Ridley. 2003. Rocks: multifunctional kinases in cell behaviour. *Nature reviews. Molecular cell biology*. 4:446-456.

Rochfort, K.D., and P.M. Cummins. 2015. The blood-brain barrier endothelium: a target for pro-inflammatory cytokines. *Biochemical Society transactions*. 43:702-706.

Scannevin, R.H., and R.L. Huganir. 2000. Postsynaptic organization and regulation of excitatory synapses. *Nature reviews. Neuroscience*. 1:133-141.

Socodato, R., C.C. Portugal, T. Canedo, I. Domith, N.A. Oliveira, R. Paes-de-Carvalho, J.B. Relvas, and M. Cossenza. 2015a. c-Src deactivation by the polyphenol 3-O-caffeoylquinic acid abrogates reactive oxygen species-mediated glutamate release from microglia and neuronal excitotoxicity. *Free radical biology & medicine*. 79:45-55.

Socodato, R., C.C. Portugal, I. Domith, N.A. Oliveira, V.S. Coreixas, E.C. Loiola, T. Martins, A.R. Santiago, R. Paes-de-Carvalho, A.F. Ambrosio, and J.B. Relvas. 2015b. c-Src function is necessary and sufficient for triggering microglial cell activation. *Glia*. 63:497-511.

Spangenberg, E.E., R.J. Lee, A.R. Najafi, R.A. Rice, M.R. Elmore, M. Blurton-Jones, B.L. West, and K.N. Green. 2016. Eliminating microglia in Alzheimer's mice prevents neuronal loss without modulating amyloid-beta pathology. *Brain*. 139:1265-1281.

Stankiewicz, T.R., and D.A. Linseman. 2014. Rho family GTPases: key players in neuronal development, neuronal survival, and neurodegeneration. *Frontiers in cellular neuroscience*. 8:314.

Thomas, R.M., C. Schmedt, M. Novelli, B.K. Choi, J. Skok, A. Tarakhovsky, and J. Roes. 2004. C-terminal SRC kinase controls acute inflammation and granulocyte adhesion. *Immunity*. 20:181-191.

Trinchese, F., S. Liu, F. Battaglia, S. Walter, P.M. Mathews, and O. Arancio. 2004. Progressive age-related development of Alzheimer-like pathology in APP/PS1 mice. *Annals of neurology*. 55:801-814.

Turrigiano, G. 2007. Homeostatic signaling: the positive side of negative feedback. *Current opinion in neurobiology*. 17:318.

Turrigiano, G.G., K.R. Leslie, N.S. Desai, L.C. Rutherford, and S.B. Nelson. 1998. Activity-dependent scaling of quantal amplitude in neocortical neurons. *Nature*. 391:892-896.

Varoqueaux, F., A. Sigler, J.-S. Rhee, N. Brose, C. Enk, K. Reim, and C. Rosenmund. 2002. Total arrest of spontaneous and evoked synaptic transmission but normal synaptogenesis in the absence of Munc13-mediated vesicle priming. *Proceedings of the National Academy of Sciences*. 99:9037-9042.

Verhage, M., A.S. Maia, J.J. Plomp, A.B. Brussaard, J.H. Heeroma, H. Vermeer, R.F. Toonen, R.E. Hammer, M. Missler, and H.J. Geuze. 2000. Synaptic assembly of the brain in the absence of neurotransmitter secretion. *Science*. 287:864-869.

Vigil, D., and C.J. Der. 2013. Inhibitors of the ROCK serine/threonine kinases: key effectors of the RhoA small GTPase. *The Enzymes*. 33 Pt A:193-212.

Wang, L., and Y. Zheng. 2007. Cell type-specific functions of Rho GTPases revealed by gene targeting in mice. *Trends in cell biology*. 17:58-64.

Wen, J., R. Ribeiro, and Y. Zhang. 2011. Specific PKC isoforms regulate LPS-stimulated iNOS induction in murine microglial cells. *Journal of neuroinflammation*. 8:38.

Wheeler, A.P., and A.J. Ridley. 2004. Why three Rho proteins? RhoA, RhoB, RhoC, and cell motility. *Experimental cell research*. 301:43-49.

Yoshizaki, H., Y. Ohba, K. Kurokawa, R.E. Itoh, T. Nakamura, N. Mochizuki, K. Nagashima, and M. Matsuda. 2003. Activity of Rho-family GTPases during cell division as visualized with FRET-based probes. *The Journal of cell biology*. 162:223-232.

Zhang, R., G. Xue, S. Wang, L. Zhang, C. Shi, and X. Xie. 2012. Novel object recognition as a facile behavior test for evaluating drug effects in AbetaPP/PS1 Alzheimer's disease mouse model. *Journal of Alzheimer's disease : JAD*. 31:801-812.

Zhou, X., and Y. Zheng. 2013. Cell type-specific signaling function of RhoA GTPase: lessons from mouse gene targeting. *The Journal of biological chemistry*. 288:36179-36188.

Figure Legends

Figure 1. Microglia-specific ablation of RhoA hampers microglia homeostasis and activates microglia in the adult brain.

A, breed scheme for inducing tamoxifen-mediated microglia-specific deletion of *RhoA* in mice. Crossing mice bearing the CreER-IRES-EYFP transgene within the Cx3cr1 locus (top) with mice in which the exon 3 of the *RhoA* gene is flanked by loxP sites (middle) gives rise to mice in which RhoA deletion in microglia is achieved by tamoxifen administration (bottom). **B**, regimen of tamoxifen (TAM) administration to CT and RhoA cKO mice and analysis of brains after 35-45 days of tamoxifen treatment. **C**, mRNA was harvested from FACS-sorted Cx3cr1-EYFP^{high} microglia from the brains of CT (RhoA$^{fl/wt}$:Cx3cr1$^{CreER/+}$) and RhoA cKO (RhoA$^{fl/fl}$:Cx3cr1$^{CreER/+}$) mice and qRT-PCR determined the abundancy of *RhoA* mRNA transcripts (n=3 animals from 2 different experiments). Graph displays means and SEM. *P<0.05 (Mann-Whitney test). **D**, microglia and macrophages in CT (RhoA$^{fl/fl}$) and RhoA cKO (RhoA$^{fl/fl}$:Cx3cr1$^{CreER/+}$) brains after 30 days of tamoxifen administration (n=5-6 animals from 2 different experiments). Graphs depict percent cell counts (mean and SEM) for each population. Cell debris was excluded by size. *P<0.05 (unpaired t test). **E,** qRT-PCR from the brains of CT (RhoA$^{fl/fl}$) and RhoA cKO (RhoA$^{fl/fl}$:Cx3cr1$^{CreER/+}$) mice after 30 days of tamoxifen administration (n=3-4 animals from 2 different experiments). Graphs (means and SEM) show the mRNA expression levels for the indicated genes. *P<0.05 (Mann-Whitney test) vs. control. **F,** qRT-PCR from FACS-sorted microglia of CT (RhoA$^{fl/wt}$:Cx3cr1$^{CreER/+}$) and RhoA cKO (RhoA$^{fl/fl}$:Cx3cr1$^{CreER/+}$) mice after 30 days of tamoxifen administration (n=3-4 animals from 2 different experiments). Graphs (means and SEM) show the mRNA expression levels for the indicated genes. *P<0.05 (Mann-Whitney test) vs. control. **G**,

confocal imaging of rat primary cortical microglial cultures transduced with pLKO (CT) or RhoA shRNA (RhoA KD). Cultures were then incubated with latex beads (green) and immunolabeled for CD11b (red). Graph (means and SEM) display mean beads/cell (n=3 different cultures). *P<0.05 (Mann-Whitney test) vs. CT. Scale bar: 20 µm.

Figure 2. Neuroinflammation in the brains of RhoA cKO mice.

A, qRT-PCR from the brains of CT ($RhoA^{fl/fl}$) and RhoA cKO ($RhoA^{fl/fl}$:$Cx3cr1^{CreER/+}$) mice after 30 days of tamoxifen administration (n=4 animals from 2 different experiments). Graphs (means and SEM) show the mRNA expression levels for the indicated genes. *P<0.05 (unpaired t test) vs. CTs. **B**, Western blot for iNOS on lysates from the brains of CT ($RhoA^{fl/wt}$:$Cx3cr1^{CreER/+}$) and RhoA cKO ($RhoA^{fl/fl}$:$Cx3cr1^{CreER/+}$) mice after 30 days of tamoxifen administration (n=5 animals from 3 different experiments). GAPDH was used as the loading control. Graphs (means and SEM) display iNOS/GAPDH ratio amounts normalized to the CT values. *P<0.05 (Mann-Whitney test) vs. CT. **C**, histological confocal analysis of GFAP immunolabeling in the cerebral cortices from CT ($RhoA^{fl/wt}$:$Cx3cr1^{CreER/+}$) and RhoA cKO ($RhoA^{fl/fl}$:$Cx3cr1^{CreER/+}$) mice after 30 days of tamoxifen administration (n=3 animals from 3 different experiments). Graphs (means and SEM) display cell counts per mm^2. *P<0.05 (paired t test). Scale bars: 50 µm.

Figure 3. Impairment of LTP and deficits in recognition memory in RhoA cKO mice.

A-C, panel (**A**) shows the averaged time course changes in field excitatory post-synaptic potential (fEPSP) slope induced by θ-burst stimulation in control ($RhoA^{fl/fl}$) and RhoA cKO ($RhoA^{fl/fl}$:$Cx3cr1^{CreER/+}$) mice 40-45 days posttamoxifen administration (n=9-10 slices pooled from 5 mice per genotype in 4 different experiments). Ordinates represent normalized fEPSP slopes, from which 0% corresponds to averaged slopes recorded for 10 min before θ-burst stimulation (-0.99±0.04 mV/ms (CT), −0.93±0.04mV/ms (RhoA cKO)), and the abscissa represents the time that average begun. Illustrative traces from representative experiments are shown in (**B**), each of which is the average of six consecutive responses obtained for CT (gray) or RhoA cKO (purple) mice before (1 or 3) and 58-60 min after (2 or 4) θ-burst stimulation, and is composed by the stimulus artifact, followed by the pre-synaptic fibre volley and the fEPSP. Panel (**C**) compares the magnitude of LTP obtained in slices from each genotype, as indicated below each bar; the values in ordinates represent the average of the fEPSP recorded 50-60 min after LTP induction, normalized to pre θ-burst stimulation values, as in (**A**). All values are presented as mean and SEM. *P<0.05 (unpaired t test) vs. CTs. **D-F**, CT ($RhoA^{fl/fl}$) and RhoA cKO ($RhoA^{fl/fl}$:$Cx3cr1^{CreER/+}$) animals were evaluated in the NOR test after 30 days of tamoxifen administration (n=7 animals from 4 different experiments). RhoA cKO mice spent more time exploring the novel object than the familiar object (**D**), whereas CT animals prefered exploring the novel object, reflecting a clear difference in the discrimination index between the genotypes (**E**). Total exploration time was similar between genotypes (**F**). Graphs (means and SEM) display the NOR parameters after a 4h delay. *P<0.05 (unpaired t test) vs. CTs.

Figure 4. Microglia-specific ablation of RhoA leads to synapse and neuronal loss.

A, Western blot for different synaptic proteins on hippocampal lysates from CT ($RhoA^{fl/fl}$) and RhoA cKO ($RhoA^{fl/fl}$:$Cx3cr1^{CreER/+}$) animals (n=3 animals). GAPDH was used as the loading control. Graphs (means and SEM) display protein of interest/GAPDH ratio normalized to the CT values. *P<0.05 (Mann-Whitney test) vs. CT. **B-D**, histological confocal analysis of vGlut-1 (green) and PSD-95 (red), pTau (red) or cleaved caspase-3 (red) immunolabeling in the hippocampus of CT ($RhoA^{fl/wt}$:$Cx3cr1^{CreER/+}$) and RhoA cKO ($RhoA^{fl/fl}$:$Cx3cr1^{CreER/+}$) mice after 30 days of tamoxifen administration (n=3 animals from 3 different experiments). Graphs are means and SEM. *P<0.05 (unpaired t test) vs. CTs. Scale bars: 5 µm and 1 µm (B); 20 µm (C); 50 µm and 10 µm (D). **E and F**, histological confocal analysis of NeuN immunolabeling in the hippocampus and neocortex from CT ($RhoA^{fl/wt}$:$Cx3cr1^{CreER/+}$) and RhoA cKO ($RhoA^{fl/fl}$:$Cx3cr1^{CreER/+}$) mice after 30 days of tamoxifen administration (n=3 animals from 3 different experiments). Graphs (means and SEM) display cell counts per mm^2. *P<0.05 (unpaired t test) vs. CTs. Scale bars: 50 µm.

Figure 5. Long-term derugulation of microglia in RhoA cKO brains.

A, regimen of tamoxifen (TAM) administration to CT and RhoA cKO mice and analysis of brains after 150-160 days of tamoxifen treatment. **B**, FACS analysis of microglia ($Ly6C^{low}CD45^{mid}CD11b^{+}$ cells) in CT ($RhoA^{fl/fl}$) and RhoA cKO ($RhoA^{fl/fl}$:$Cx3cr1^{CreER/+}$) brains after 150-160 days of tamoxifen administration (n=5 animals from 2 different experiments). Graphs depict microglial cell counts (mean and SEM). Cell debris was excluded by size. *P<0.05 (unpaired t test) vs. CT. **C**, qRT-PCR from the brains of CT ($RhoA^{fl/fl}$) and RhoA cKO ($RhoA^{fl/fl}$:$Cx3cr1^{CreER/+}$) mice after 150-160 days of tamoxifen administration (n=10-11 animals from 3 different experiments). Graphs (means and SEM) show the mRNA expression levels for the indicated genes *P<0.05 (unpaired t test) vs. CTs.

Figure 6. Activation of microglia by LPS or hypoxia requires decrease of RhoA activity.

A, RhoA pull down in control (CT) and LPS (1 µg/ml; 1 h)-treated primary rat cortical microglial cultures (n=3 different cultures). Gels display immunoblots for RhoA in GTP-bound (active RhoA) or input (total lysates) fractions. **B**, primary rat cortical microglia expressing the Raichu-RhoA FRET biosensor were exposed to 1 µg/ml LPS (n=5 cells pooled across 3 different cultures). Panels show time-lapse FRET/CFP images coded according to the pseudocolor ramp. FRET/CFP ratio changes were normalized at 0 min and plotted. Scale bar: 10 µm. **C and D**, CHME3 microglia expressing the Raichu-RhoA FRET biosensor were subjected to hypoxia (2% O_2/5% CO_2; **C**) or treated with IL-4 (10 ng/ml; **D**). Panels show time-lapse FRET/CFP images coded according to the pseudocolor ramp (n=5 cells pooled across 3 different cultures). FRET/CFP ratio changes were normalized at 0 min and plotted. Scale bars: 10 µm. **E and F**, CHME3 microglia expressing the HSP ROS FRET biosensor were transfected with the $RhoA^{Q63L}$ construct (purple circles) or with the mock control (dark grey circles) and then exposed to LPS (1 µg/ml; **E**) or subjected to hypoxia (2% O_2/5% CO_2; **F**). Panels show time-lapse FRET/CFP images coded according to the pseudocolor ramp (n=5 cells for each condition pooled across 3 different cultures). FRET/CFP ratio changes were normalized at 0 min and plotted. Scale bars: 10 µm.

Figure 7. RhoA depletion modulates Csk/Src pathway in microglia.

A, qRT-PCR from FACS-sorted microglia of CT ($RhoA^{fl/wt}$:$Cx3cr1^{CreER/+}$) and RhoA cKO ($RhoA^{fl/fl}$:$Cx3cr1^{CreER/+}$) mice after 30 days of tamoxifen administration (n=3-4 animals from 2 different experiments). Graphs (means and SEM) show the mRNA expression levels for Csk. *P<0.05 (Mann-Whitney test) vs. control. **B**, Western blot for Csk on lysates from control (CT) or RhoA shRNA (RhoA KD) stable N9 microglial cell sub-clones (n=3 different cultures). Actin was used as the loading control. Graphs (means and SEM) display Csk/Actin ratio normalized to the CT values. *P<0.05 (Mann-Whitney test) vs. CT. **C**, confocal imaging of rat primary cortical microglial cultures transduced with pLKO (CT) or RhoA shRNA (RhoA KD) and immunolabeled for Csk (green) and CD11b (red). Graph (means and SEM) display Csk mean fluorescence intensity normalized to the CT (n=3 different cultures). *P<0.05 (Mann-Whitney test) vs. CT. Scale bar: 20 µm. **D**, histological confocal analysis of CT ($RhoA^{fl/wt}$:$Cx3cr1^{CreER/+}$) and RhoA cKO ($RhoA^{fl/fl}$:$Cx3cr1^{CreER/+}$) mice after 30 days of tamoxifen administration (n=22-39 cells from 3 mice per genotype pooled across 2 different experiments). Src $pTyr^{416}$ (red) and GFP (green) immunolabeling on tissue sections from the cerebral cortex are shown. Graph (mean and SEM) depicts Src $pTyr^{416}$ intensity per GFP^{+} cells. *P<0.0001 (unpaired t test) vs CT. Scale bar: 50 µm. **E**, Western blot for Src $pTyr^{416}$ on lysates from control (CT) or RhoA shRNA (RhoA KD) stable N9 microglial cell sub-clones (n=3 different cultures). Src was used as the loading control. Graphs (means and SEM) display Src $pTyr^{416}$/Src ratio normalized to the CT values. *P<0.05 (Mann-Whitney test) vs. CT. **F**, CHME3 microglial cultures expressing the c-Src FRET biosensor (KRas Src YPet) were infected with control (CT) or RhoA shRNA (RhoA KD) lentiviruses (n=16-18 cells pooled across 3 different experiments). Graph (means and SEM) displays time-lapse CFP/FRET ratio images averaged for 10 min. Pseudocolor ramps represent

min/max CFP/FRET ratios. *P<0.05 (Mann-Whitney test) vs. CT. Scale bar: 5 µm. **G and H**, Western blot for Csk (E) or Src pTyr^{416} (F) on lysates from N9 microglial cells transfected with the RhoA Q63L mutant and treated with LPS (1 µg/ml; 24 h) or subjected to hypoxia (2% O_2/5% CO_2). Actin (E) and Src (F) were the loading controls (n=3-4 different cultures). Graphs (means and SEM) display Csk/actin (E) and Src pTyr^{416}/Src (F) ratios normalized to the CTs values. *P<0.05, **non-significant (One-way ANOVA). **I**, CHME3 microglia expressing the KRas Src FRET biosensor were transfected with RhoA^{Q63L} or not (mock) and subjected to hypoxia (2% O_2/5% CO_2). Panels show time-lapse CFP/FRET images coded according to the pseudocolor ramp (n=5 cells pooled across 2 different experiments). Scale bars: 10 µm. **J-L,** confocal imaging of p65-GFP-transfected (green; **J**) pLKO, Csk KD or Src^{Y527F} stable N9 microglial cell sub-clones. Nuclei were stained with DAPI (blue). TNF (ELISA; **K**) and glutamate content (fluorimetry; **L**) were determined from the culture media. Graphs are mean and SEM (n=3-4 cultures from 2 different experiments). *P<0.05 (Kruskal-Wallis test with Dunn`s post-hoc analysis) vs. CTs. Scale bar: 10 µm.

Figure 8. RhoA controls microglia homeostasis and recognition memory through Src activity.

A, regimen of AZD 0530 or DMSO injections (1 IP per week during 4 weeks) to RhoA cKO mice after TAM administration. **B**, FACS analysis of microglia in RhoA cKO mice injected with DMSO (purple dots) or AZD 0530 (red dots) (n=4-5 animals from 3 different experiments). Graphs depict microglia cell counts (mean and SEM). Dashed line displays the mean microglial cell number in CT ($RhoA^{fl/fl}$) brains. *P<0.05 (Mann-Whitney test) vs. RhoA cKO. **C**, qRT-PCR from the brains of RhoA cKO mice injected with DMSO (purple dots) or AZD 0530 (red dots) (n=5-9 animals from 3 different experiments). Graphs (means and SEM) show the transcript abundance for the indicated genes. Dashed lines display the mean mRNA levels for the indicated transcripts in CT ($RhoA^{fl/fl}$) brains. *P<0.05, **P<0.01, ***P<0.001 (unpaired t test) vs. RhoA cKO. **D,** Western blot for synaptophysin or PSD-95 on hippocampal lysates from RhoA cKO mice injected with DMSO (purple dots) or AZD 0530 (red dots) (n=6-9 animals from 3 different experiments). GAPDH was used as the loading control. Graphs (means and SEM) display protein of interest/GAPDH ratio normalized (dashed lines) to values obtained from $RhoA^{fl/fl}$ animals. *P<0.05 (Mann-Whitney test) vs. RhoA cKO. **E-G**, DMSO (purple dots) and AZD 0530-injected (red dots) RhoA cKO mice were evaluated in the NOR test (n=4-9 animals from 3 different experiments). AZD-injected mice performed the NOR test substantially better than DMSO-injected mice. AZD-injected RhoA cKO animals also explored more the novel object (**E**) and had an overall improvement in recognition index when compared with DMSO-injected RhoA cKO animals (**F**). Total exploration time was similar in both genotypes (**G**). Graphs (means and SEM) display the NOR parameters after a 4h delay. Dashed lines display the average behaviour of CT ($RhoA^{fl/fl}$) animals for the indicated parameters. *P<0.05 (unpaired t test) vs. RhoA cKO.

Figure 9. Control of gatekeeper function of microglia by RhoA.

A, steady state microglial RhoA signaling sustains Csk abundance to control basal Src activity, restraining the microglia proinflammatory activation and deregulation of microglial phagocytosis. Microglia expressing RhoA critically contribute for the normal triggering of LTP and recognition memory.

B, ablation of microglial RhoA downregulates Csk and overactivates Src, leading to proinflammatory microglia polarization and increased microglia phagocytosis. As a consequence, microglia-specific deletion of RhoA culminates in a degenerative brain pathology primarily mediated by microglial activation.

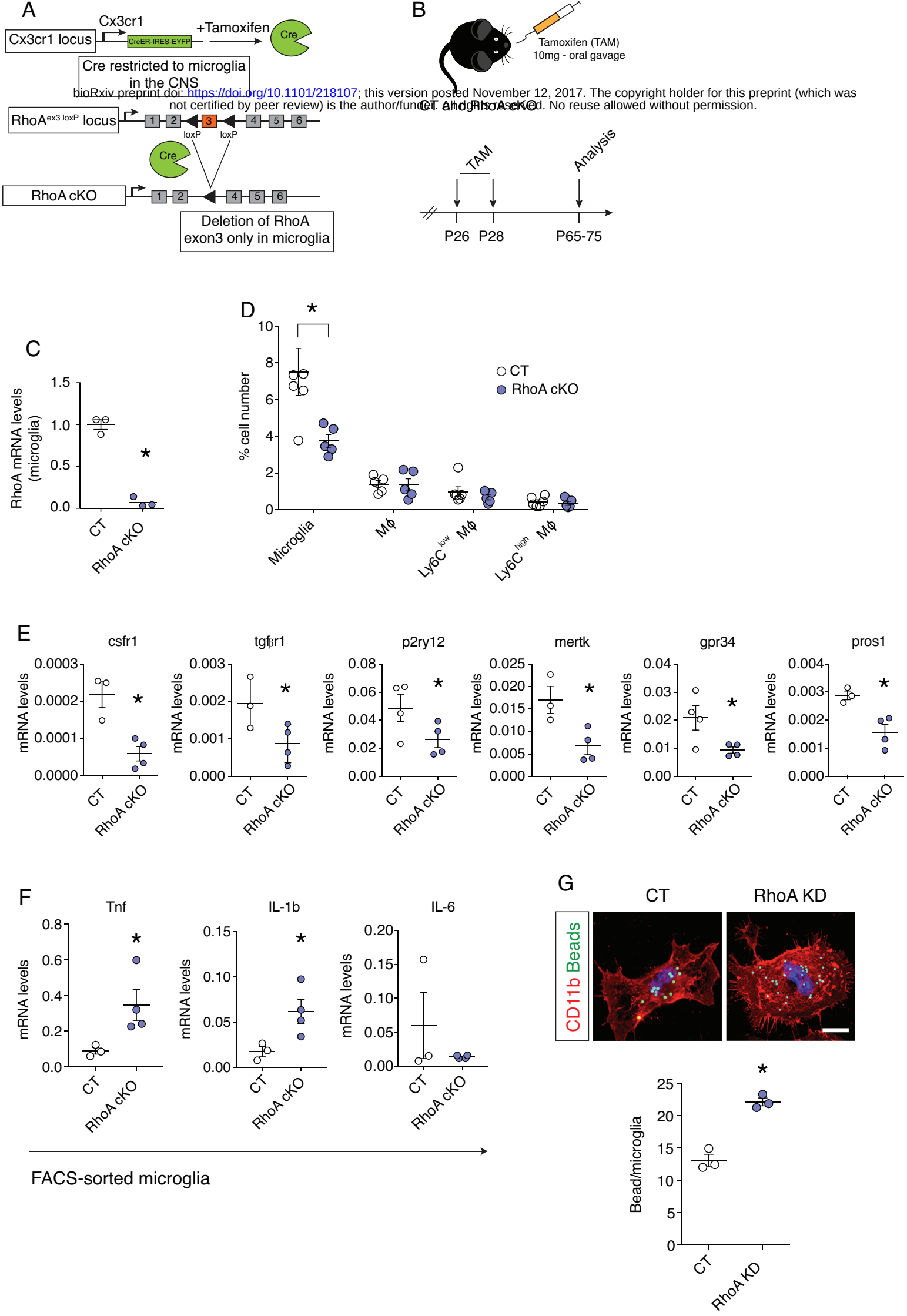

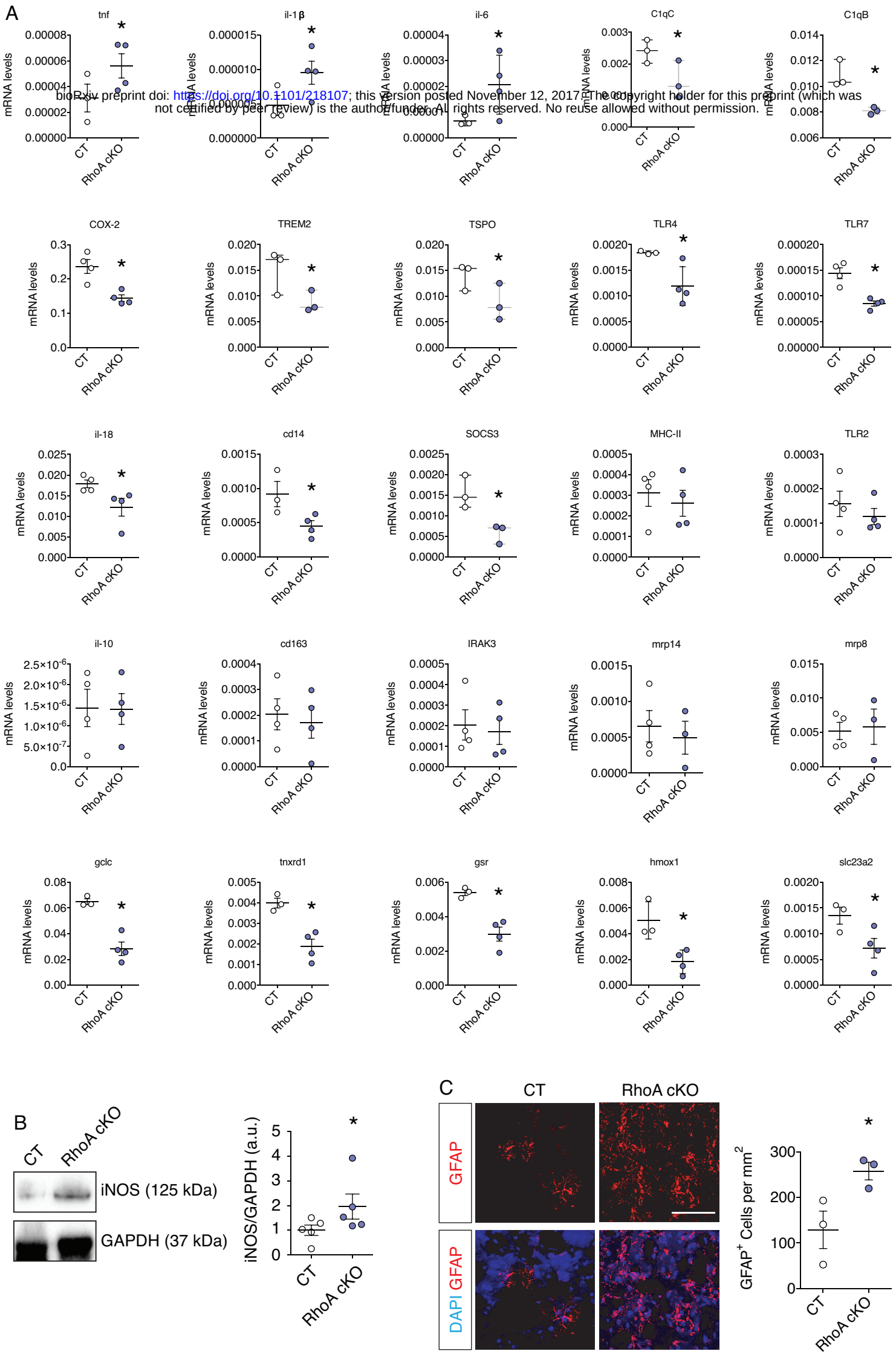

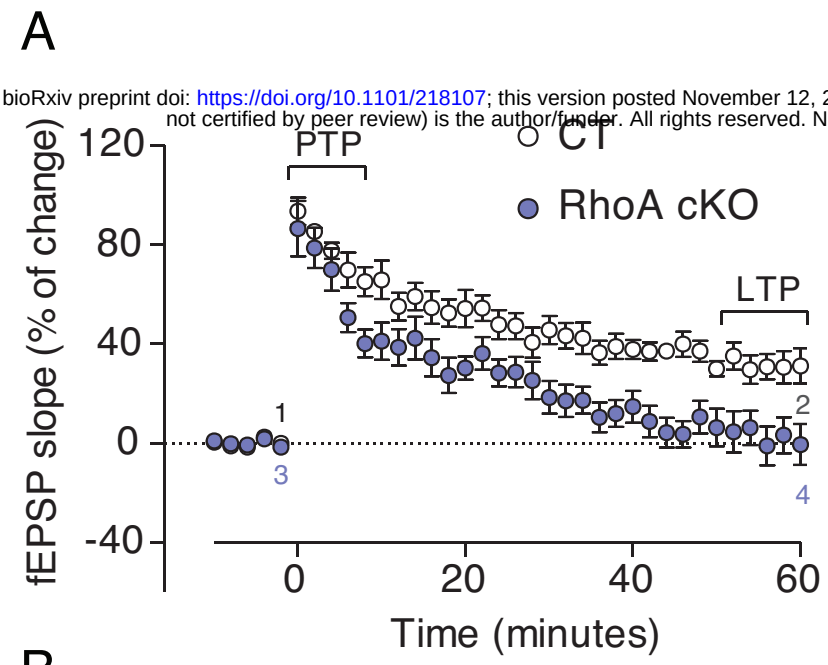

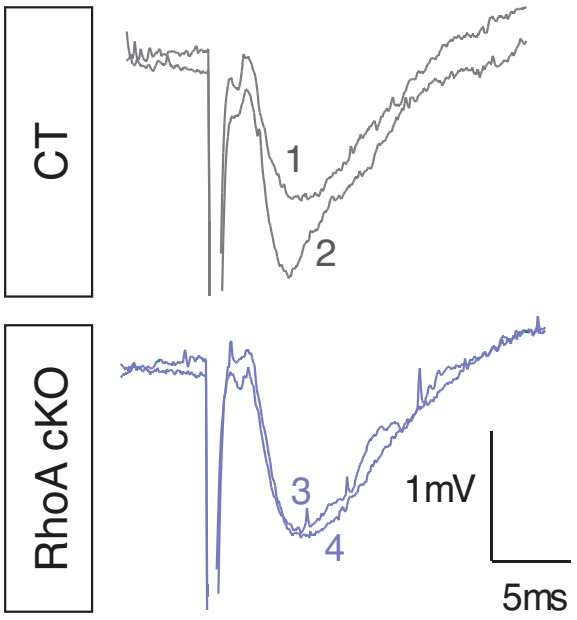

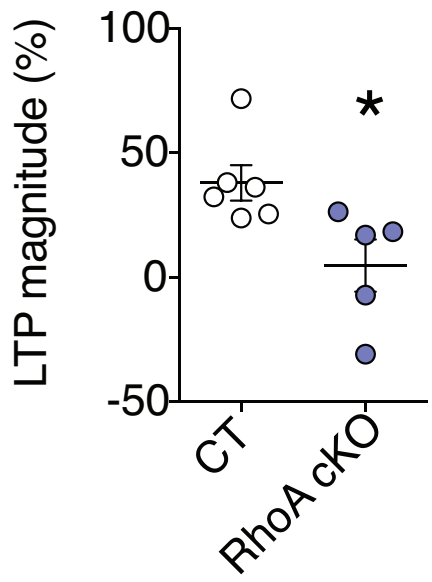

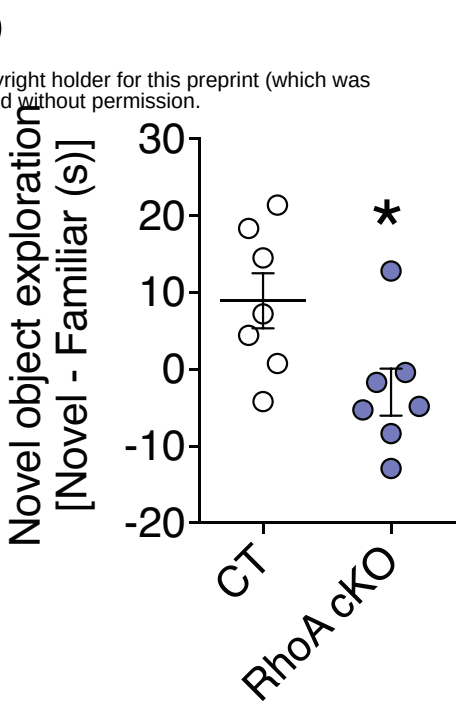

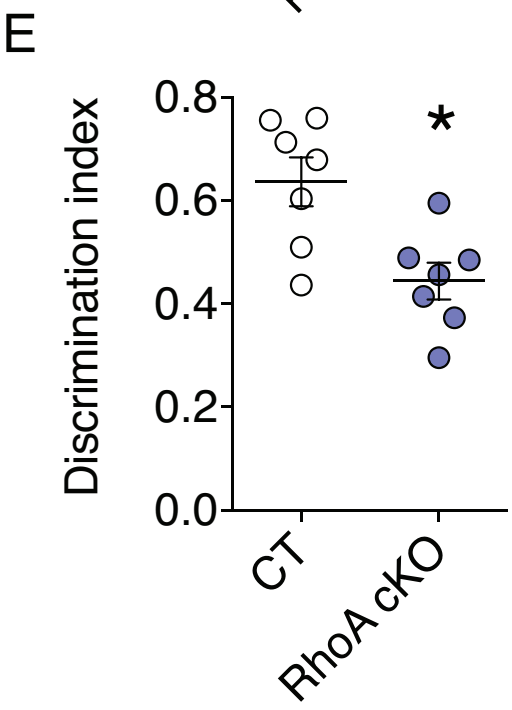

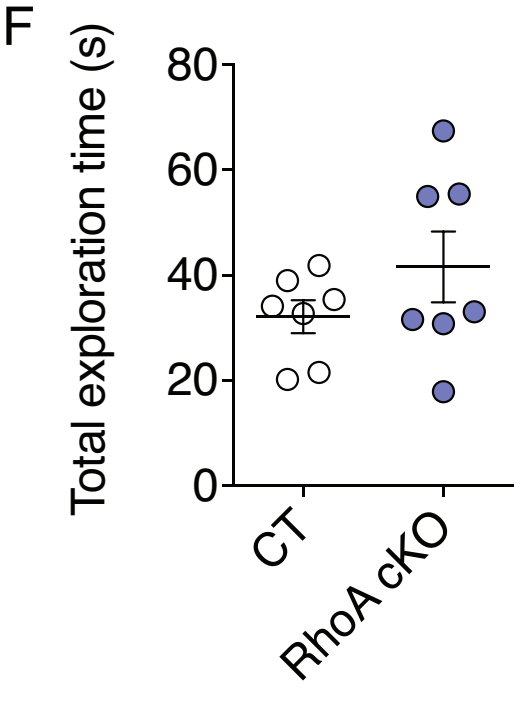

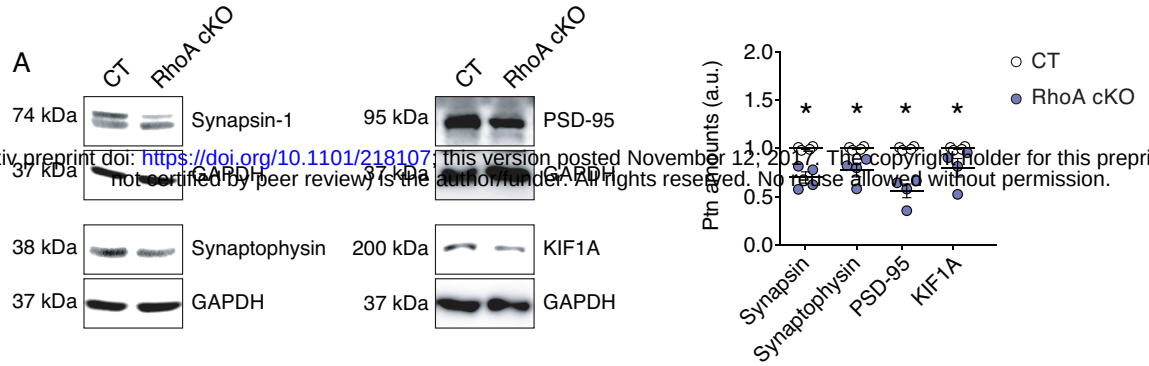

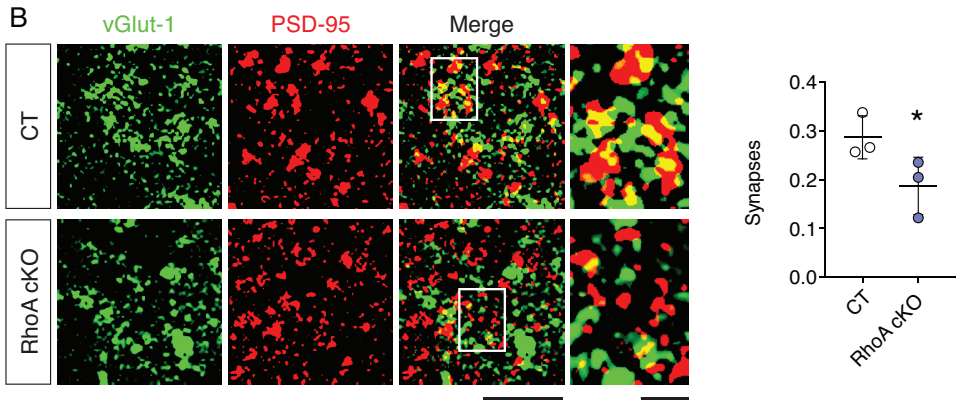

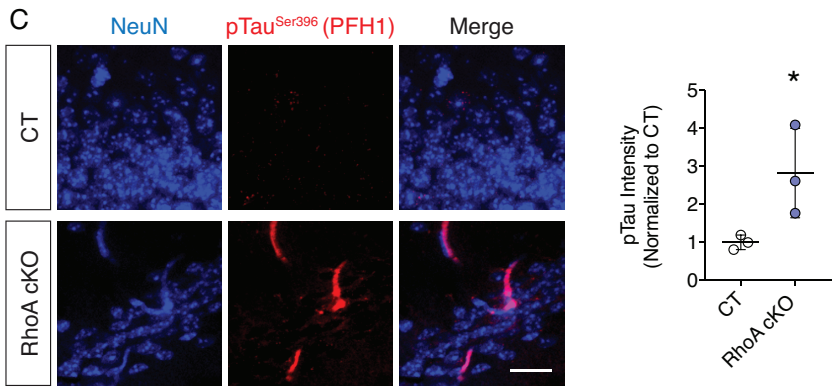

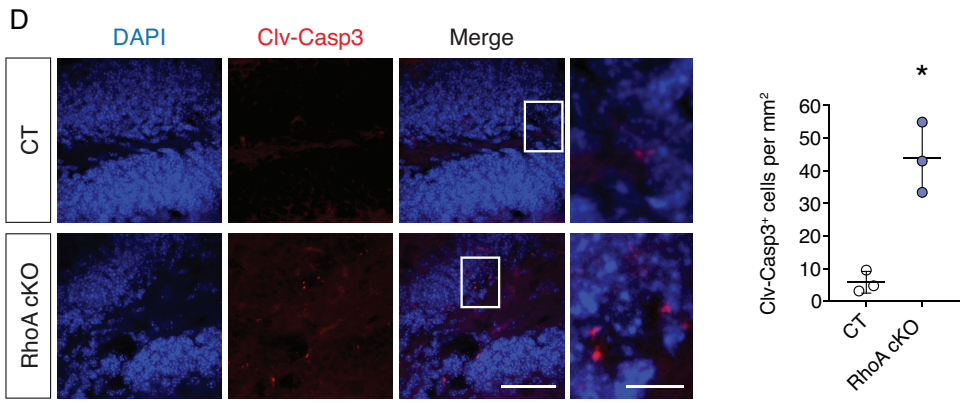

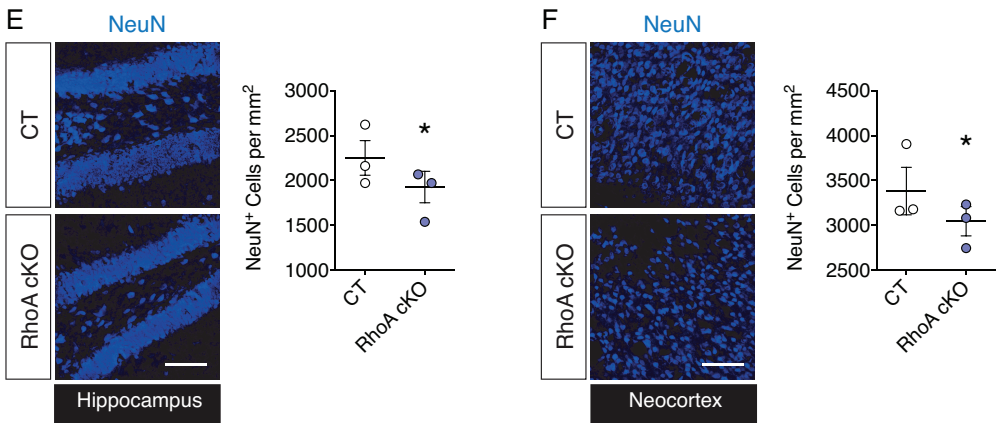

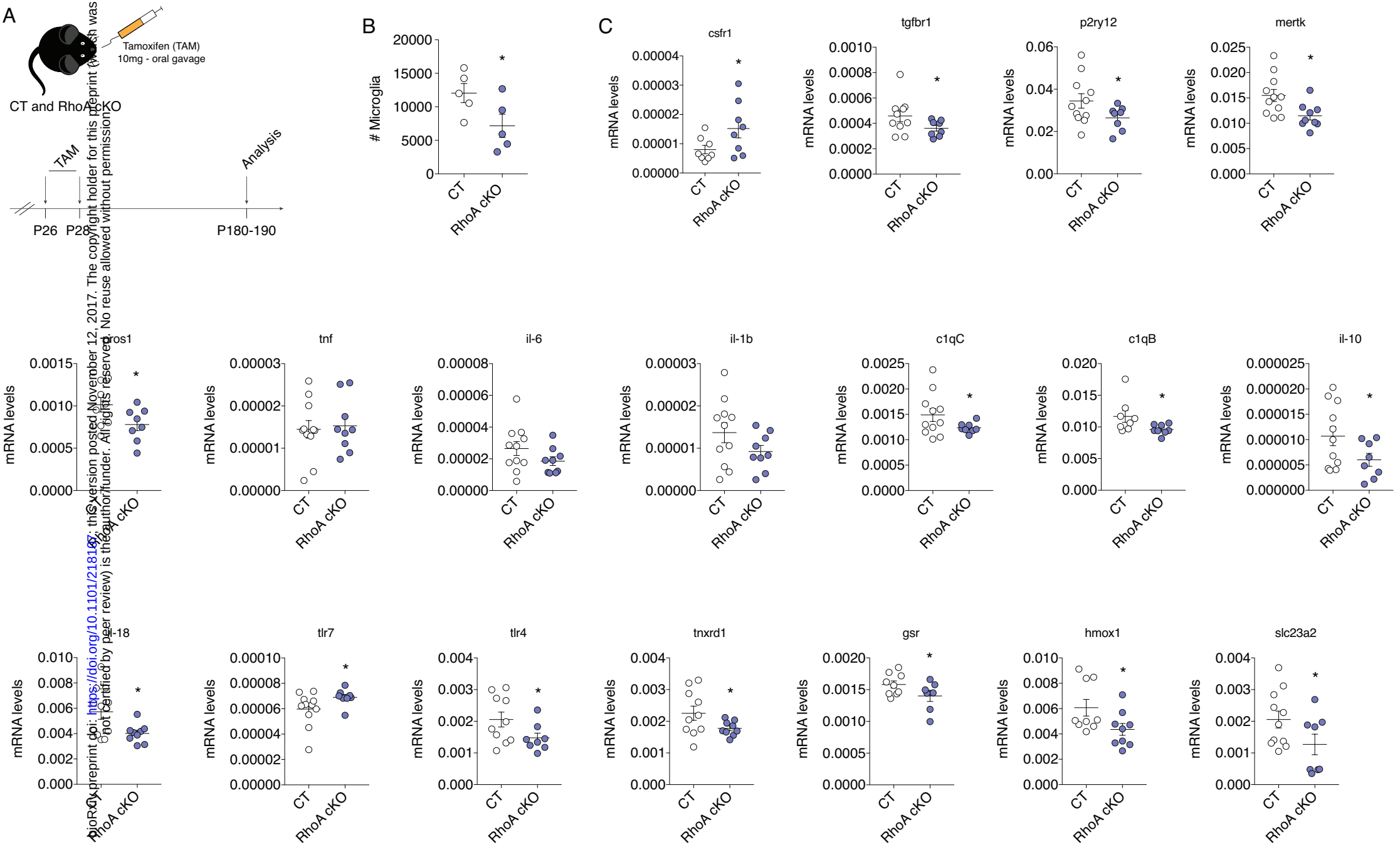

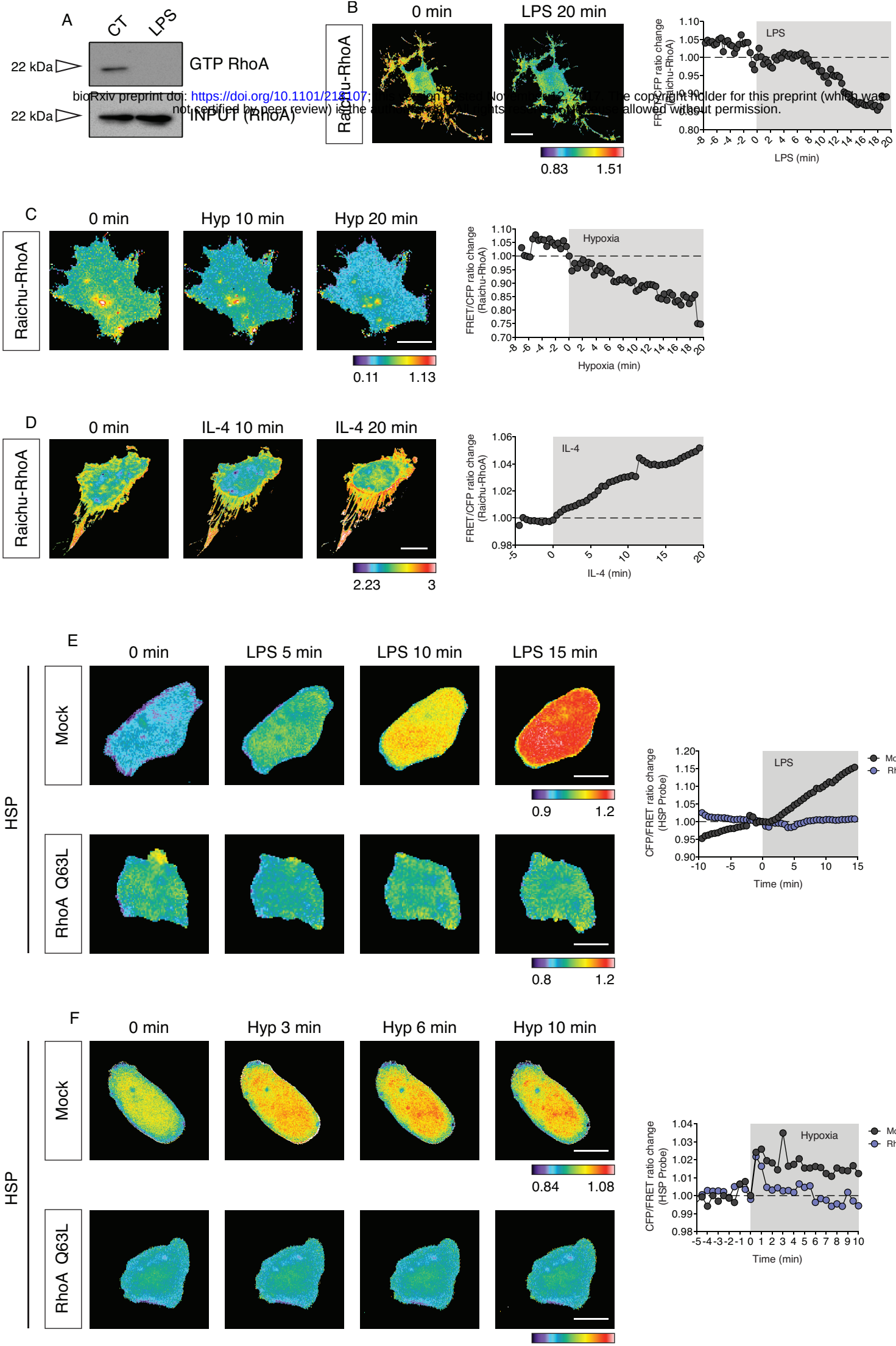

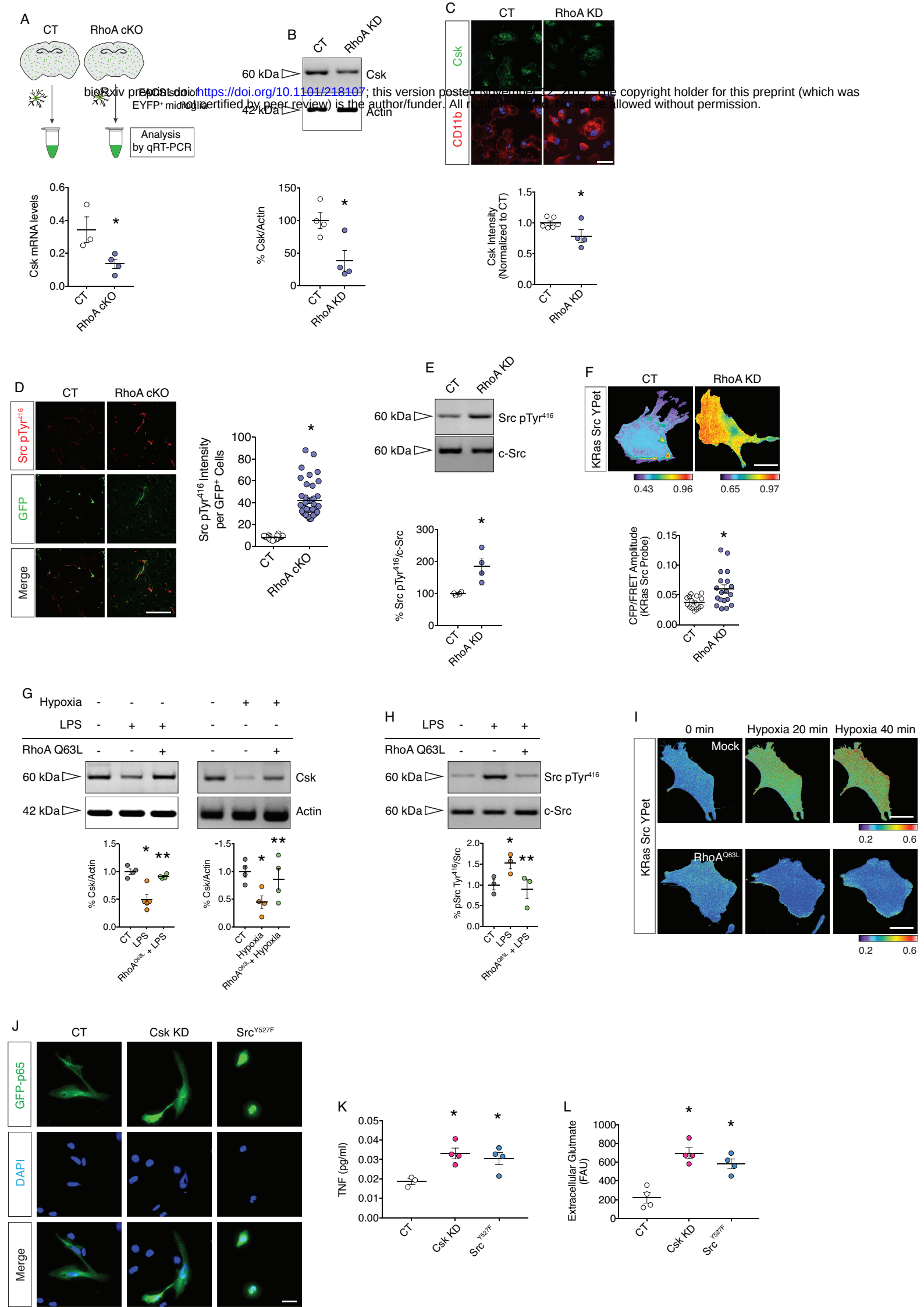

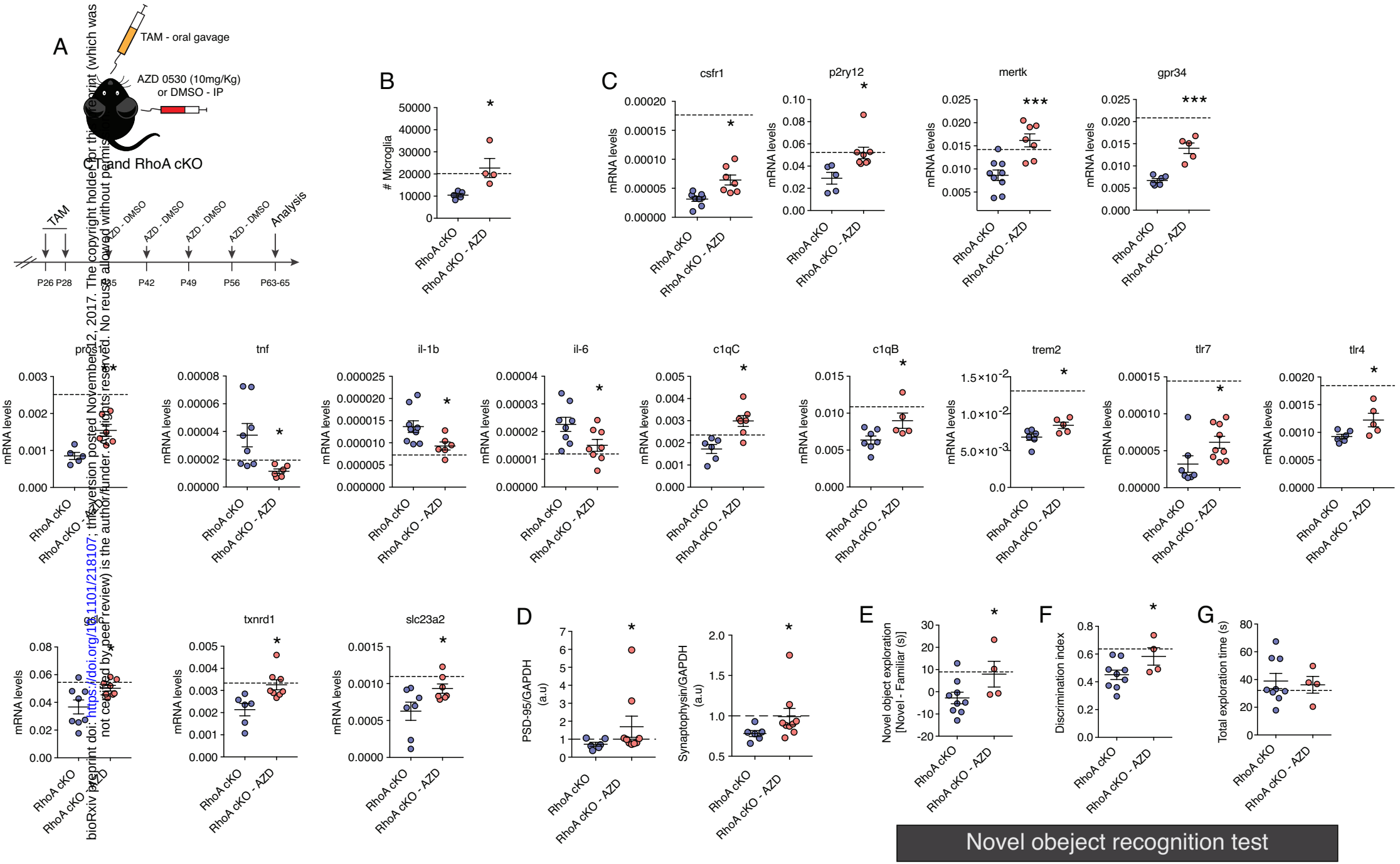

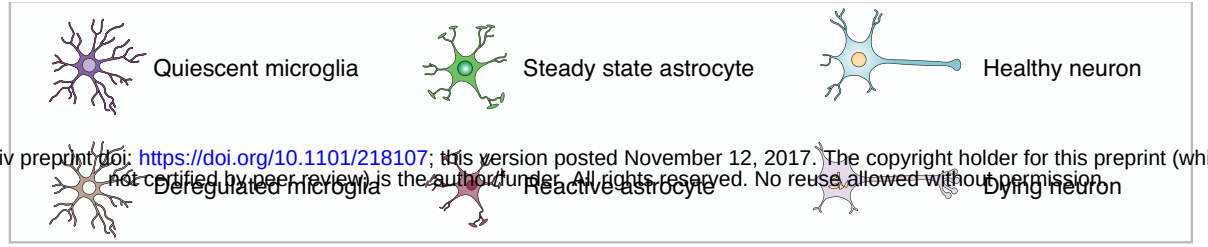

A. Brain architecture with microglia expressing RhoA

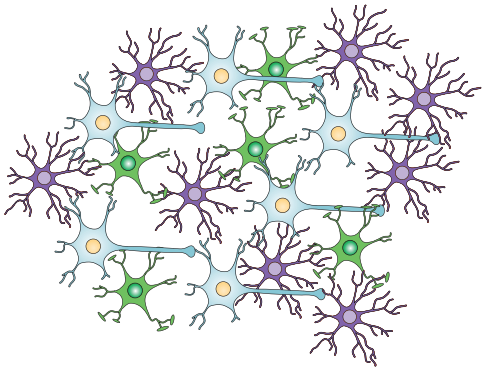

RhoA — Active RhoA

↓

Csk — Steady state Csk amounts

⊣

Src — Basal Src activity

↓

Low inflammation
Low oxidative stress
Balanced phagocytosis

↓

Monitoring of synapses
Maintenance of neuronal health
Fine-tuning of plasticity and behaviour

↓

Normal brain functioning

B. Brain architecture with microglia lacking RhoA

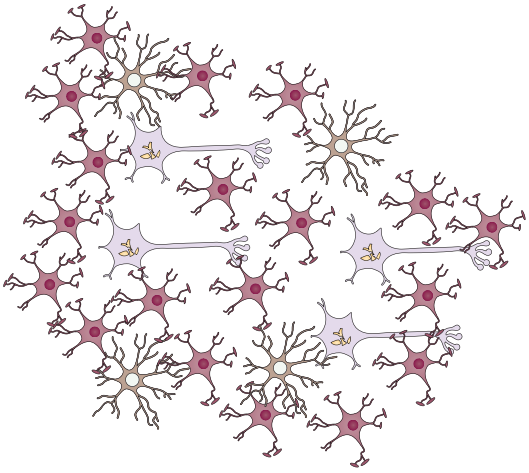

RhoA — Loss of RhoA

⊣

Csk — Downregulation of Csk

⇓

Src — Overactivation of Src

↓

Inflammation
Oxidative burden
Deregulated phagocytosis

↓

Loss of synapses
Triggereing of neuronal death
Impairment of plasticity and behaviour

↓

Degenerative brain pathology